

**g-C₃N₄ Decorated with Hydrogen Peroxide Modified Titania
and Bismuth Vanadate for Enhanced Photocatalytic
Degradation of Aqueous Methyl Orange Dye**



MASTERS OF PHILOSOPHY

In

Environmental Sciences

By

Waqar Alam

Resgistration No# 02312113012

Department of Environmental Sciences

Faculty of Biological Sciences

Quaid-i-Azam University

Islamabad, Pakistan

2021-2023

**g-C₃N₄ Decorated with Hydrogen Peroxide Modified Titania
and Bismuth Vanadate for Enhanced Photocatalytic
Degradation of Aqueous Methyl Orange Dye**



MASTERS OF PHILOSOPHY

In

Environmental Sciences

By

Waqar Alam

Resgistration No# 02312113012

Department of Environmental Sciences

Faculty of Biological Sciences

Quaid-i-Azam University

Islamabad, Pakistan

2021-2023

Plagiarism Undertaking

I, **Waqar Alam**, hereby state that my M.Phil. Thesis titled “**g-C₃N₄ Decorated with Hydrogen Peroxide Modified Titania and Bismuth Vanadate for Enhanced Photocatalytic Degradation of Methyl Orange Dye**” is solely my research work with no significant contribution from any other person. Small contribution/help whatever is taken has been duly acknowledged and that complete thesis has been written by me.

I understand the zero-tolerance policy of the HEC and Quaid-I-Azam University, Islamabad, towards plagiarism. Therefore, I as an author of the above-titled thesis declare that no portion of my thesis has been plagiarized and any material used as reference is properly referred/cited.

I undertake that if I am found guilty of any form of plagiarism in the above-titled thesis even after the award of my M.Phil. degree, the university reserves the right to withdraw/revoke my M.Phil. degree and that HEC and the university have the right to publish my name on the HEC/University website on which the names of students are placed who submitted plagiarism.

Waqar Alam

Author's Declaration

I **“Waqar Alam (Reg. No. 02312113012)”** hereby state that my M.Phil. thesis titled **“g-C₃N₄ Decorated with Hydrogen Peroxide Modified Titania and Bismuth Vanadate for Enhanced Photocatalytic Degradation of Methyl Orange Dye”** was carried out by me in the Catalysis for Environment and Energy Laboratory, Department of Environmental Sciences, Quaid-i-Azam University, Islamabad. The results, findings, conclusions, and investigations of this research have not been previously presented and published as research work in any other university.

Waqar Alam

Reg No. 02312113012

APPROVAL CERTIFICATE

It is to certify that the research work presented in this thesis, entitled "g-C₃N₄ decorated with Hydrogen Peroxide Modified Titania and Bismuth Vanadate for Enhanced Photocatalytic Degradation of Aqueous Methyl Orange Dye" was conducted by **Mr. Waqar Alam** (Reg. No. 02312113012) under the supervision of **Dr. Jamshaid Rashid**. No part of this thesis has been submitted else for any other degree. This thesis is submitted to the **Department of Environmental Sciences**, in the partial fulfillment of the requirements for the degree of **Master of Philosophy in the field of Environmental Sciences**, Department of Environmental Sciences, Quaid-i-Azam University Islamabad, Pakistan.

Mr. Waqar Alam (MPhil Scholar)


Supervisor:

Dr. Jamshaid Rashid

Associate Professor

Department of Environmental Sciences

Quaid-i Azam University, Islamabad



External Examiner:

Dr. Qaisar Hussain

Associate Professor

Soil Science and Soil Water Conservation

Department PMAS Arid Agriculture University, Rawalpindi



Chairperson:

Dr. Abida Farooqi

Professor

Department of Environmental Sciences

Quaid-i Azam University, Islamabad



Table of Contents

Acknowledgment	i
List of Abbreviations	ii
List of Tables	iv
List of Figures	v
Abstract	vii
1.1. Impact of Textile Industry on Water Resources	2
1.2. Industrial dyes: An Overview	3
1.3. Historical use of Dyes	4
1.4. Toxicity of Dyes.....	5
1.5. Impacts of Dyes on Human Health	8
1.6. Distinguishing Between Dyes and Pigments	8
1.7. Chemical Nature of Dyes	9
1.8. Colour of Dyes.....	9
1.9. Types of Dyes	10
1.9.1. Natural Dyes	10
1.9.2. Mordants	11
1.9.3. Synthetic Dye	11
1.10. Characteristics of Azo Dyes.....	13
1.10.1. Methyl Orange (MO)	13
1.11. Conventional Methods used for Treating Textile Effluent.....	15
1.12. Approaches for Mineralization of MO	18
1.12.1. Heterogeneous Photocatalysis	18
1.13. Nanoparticles and Photocatalytic Properties	20
1.13.1. Bismuth Vanadate Nano-powders.....	21
1.13.2. Hydrogen Peroxide Modified Titania Powders.....	23

1.13.3.	Graphitic Carbon Nitride (g-C ₃ N ₄)	24
1.14.	Problem Statement	26
1.15.	Aims and Objectives	26
1.16.	Significance of the study	26
2.	METHODOLOGY	28
2.1.	Materials	28
2.2.	Instruments.....	28
2.3.	Experimental Procedures	28
2.3.1.	Preparation of Photocatalysts	28
2.3.2.	Synthesis of BiVO ₄	28
2.3.3.	Synthesis of Hydrogen Peroxide Modified Titania	29
2.3.4.	Synthesis of Graphitic Carbon Nitride	30
2.3.5.	Figure 2.3: Flow chart of synthesis of graphitic carbon nitride (g-C ₃ N ₄)Preparation of Binary Composite	30
2.3.6.	Preparation of Ternary Composite.....	31
2.4.	Photocatalytic Experiments	32
2.4.1.	Optimization Studies	32
2.4.2.	Catalytic dose Experiments	32
2.4.3.	Point of Zero Charge	32
2.4.4.	pH of Solution Experiment.....	33
2.4.5.	Concentration of Solution Experiment.....	33
2.4.6.	Characterizations	33
3.	RESULTS AND DISCUSSION	35
3.1.	Characterization Results of Nanocatalysts.....	35
3.1.1.	X-ray Diffraction	35
3.1.2.	Morphological Assessment of Nano-catalyst	36
3.1.3.	Elemental Composition Analysis.....	38

Figure 3.4: EDS spectrum of 15% ternary composite (BiVO ₄ @HMT/g-C ₃ N ₄).	39
3.1.4. Optical Properties and Band Gap Analysis.....	39
3.2. Calibration Curve of Methyl Orange	40
3.3. Preliminary Studies	41
3.4. Optimization Studies.....	43
3.4.1. Point of Zero Charge	43
3.4.2. Effect of Solution pH.....	44
3.4.3. Effect of pollutant concentration	45
3.4.4. Effect of Photo-Catalyst Dose	46
3.4.5. Reusability.....	47
CONCLUSION	54
REFERNCES	55

Acknowledgment

In the name of ALLAH Almighty, the Most Merciful and Beneficent, the One who has bestowed upon me His boundless blessings and granted me the strength to successfully complete this endeavor. Peace and blessings be upon the Prophet Muhammad (PBUH), the illuminator of humanity's path from darkness to light.

Foremost, I extend my deepest gratitude to my esteemed supervisor, Dr. Jamshaid Rashid, Associate Professor in the Department of Environmental Sciences at Quaid-i-Azam University, Islamabad. His unwavering guidance and unwavering support were indispensable in the realization of this work.

I cannot express enough gratitude to my beloved family, my parents, and sisters whose boundless love, sacrifices, and unwavering belief in me have been the cornerstone of my journey.

To my Lab mates Fatima Imtiaz, and Ayesha Arif for your support. I also extend my sincere appreciation to my friends Zoha Zehra, Hussain Ahmed, Areej Arif, and M. Maaz, whose friendship and encouragement added a special dimension to my MPhil journey.

I extend my gratitude and love to Zoha Zahid for support throughout the two years.

Waqar Alam

List of Abbreviations

°C	Degrees Celsius
AOPs	Advanced Oxidation Processes
BC	Binary Composite
BiVO ₄	Bismuth Vanadate
CB	Conduction Band
EDS	Energy Dispersive X-ray Spectroscopy
g/L	Gram per Liter
g-C ₃ N ₄	Graphitic Carbon Nitride
h	Hour
H ₂ O ₂	Hydrogen Peroxide
HMT	Hydrogen peroxide-Modified Titania
HOMO	Molecule's Highest Occupied Molecular Orbital
JCDPS	Joint Committee on Powder Diffraction Standards
LUMO	Lowest Unoccupied Molecular Orbital
MB	Methyl Blue
min	Minute
MO	Methyl Orange
NPs	Nanoparticles
PCRWR	Pakistan Council of Research in Water Resources
SDGs	Sustainable Development Goals
SEM	Scanning Electron Microscopy
TC	Ternary Composite
TEM	Transmission Electron Microscopy
TiO ₂	Titanium dioxide
UNO	United Nations Organization
UV	Ultraviolet
VB	Valence Band
VLA	Visible Light Active
VLD	Visible Light Driven
VLR	Visible Light Responsive

WHO

World Health Organization

WRI

Water Resource Institute

XRD

X-ray Diffraction

List of Tables

Table 3.1: Comparison between pseudo first order, second order and Pseudo First kinetics applied on different operational parameters.....	52
Table 3.2: Comparison of catalyst activities for MO dye degradation from literature.....	54

List of Figures

Figure 0.1: Schematic illustration of dye pollution sources, sink and effects. Source (Ayele et al., 2021).....	7
Figure 0.2: Classification of dyes based on their nature. Source: (Uddin & Rehman, 2018)	13
Figure 0.3: Chemical structure of Methyl Orange dye. Source: (Regraguy et al., 2022).....	14
Figure 0.4: Effect of acidic and basic media on the Colour change of MO. Source: (Malviya et al., 2015).....	14
Figure 0.5: Schematic diagram of treatment methods for textile wastewater. Source (Azanaw et al., 2022).....	15
Figure 0.6: Prospective applications of photocatalysis. Source: (Tatarchuk et al., 2018).....	19
Figure 0.7: Schematic diagram of heterogeneous photo catalysis.....	20
Figure 0.8: Crystalline phases of BiVO ₄ . Source: (Anusuyadevi., 2018)	23
Figure 0.9: Structure of melamine and graphitic carbon nitride. Sources (Zhang et al., 2013)	26
Figure 2.1: Scheme for synthesis of BiVO ₄	29
Figure 2.2 : Flow diagram of synthesis of HMT	30
2.3.5. Figure 2.3: Flow chart of synthesis of graphitic carbon nitride (g-C ₃ N ₄)Preparation of Binary Composite	30
Figure 2.4: Synthesis of fractions of binary composite (BiVO ₄ /HMT)	31
Figure 3.1: XRD patterns of BiVO ₄ , g-C ₃ N ₄ , HMT, and 15% (BiVO ₄ @HMT/g-C ₃ N ₄).....	36
Figure 3.2: (a) SEM image of BiVO ₄ , (b) SEM image of gC ₃ N ₄ , (c) SEM image of HMT, (d) SEM image of 15% (BiVO ₄ @ HMT/gC ₃ N ₄) ternary composite.....	38
Figure 3.3: TEM image of Ternary Composite (BiVO ₄ @HMT/g-C ₃ N ₄).....	38
Figure 3.4: EDS spectrum of 15% ternary composite (BiVO ₄ @HMT/g-C ₃ N ₄).	39
Figure 3.5: (a) UV-visible absorbance spectra of pure BiVO ₄ , g-C ₃ N ₄ , and 15% BiVO ₄ @HMT/g-C ₃ N ₄ ; (b) Tauc plot of BiVO ₄ , g-C ₃ N ₄ , and 15% BiVO ₄ @HMT/g-C ₃ N ₄	40
Figure 3.6: Calibration Curve of Methyl Orange Dye standards	40
Figure 3.7: Degradation of MO using pure BiVO ₄ , HMT, g-C ₃ N ₄ , and photolysis	41
Figure 3.8: Percentage degradation of MO by binary composite (BiVO ₄ @HMT) fractions.....	42
Figure 3.9: Degradation of MO over ternary composite (BiVO ₄ @HMT/g-C ₃ N ₄)	43
Figure 3.10: Point of zero charge of 15% ternary composite.	44
Figure 3.11: Effect of pH on degradation of methyl orange under visible light.....	45

Figure 3.12: Effect of pollutant concentration on degradation of MO under visible light using 15% BiVO ₄ @HMT/g-C ₃ N ₄ at pH 5.	46
Figure 3.14: Reusability of 15% TC for photo degradation of MO	48
Figure 3.15: Photodegradation kinetic plot showing the effect of binary composite loading (catalyst dose = 1g/L, MO concentration = 25mg/L).....	50

Abstract

The discharge of dye-contaminated wastewater, particularly azo dyes like methyl orange, poses a significant environmental concern, adversely affecting water bodies, ecosystems, and public health. Conventional treatment methods, marred by the production of secondary pollutants and inefficient dye removal, underscore the need for innovative and sustainable alternatives. This study aims to explore a novel approach utilizing ternary composite photocatalyst (15% BiVO₄@HMT/g-C₃N₄) for the degradation of methyl orange (MO) under visible light irradiation. Synthesized catalysts were characterized by analytical techniques like X-ray diffraction, Energy dispersive X-ray spectroscopy, scanning electron microscopy and transmission electron microscopy, which confirmed the formation of pure crystalline structures, perfect elemental composition of BiVO₄, HMT and 15% BiVO₄@HMT/g-C₃N₄ powders, without incorporation of any impurities. Optical properties of as prepared catalysts were tested with UV-visible diffuse reflectance spectroscopy. Preliminary testing of pristine photocatalysts (BiVO₄, hydrogen peroxide-modified titania (HMT), and g-C₃N₄), as well as binary and ternary composites was carried out. The superior performance of the ternary composite prompted its selection for further experimentation. Optimization studies were conducted to identify the optimal pH, dose, and concentration of the solution for effective methyl orange degradation. The ternary composite is demonstrated to degrade methyl orange up to 79.32%. Additionally, its reusability is evidenced by consistent performance across three cycles, with the third cycle showing approximately 70% degradation efficiency. Degradation reaction rates were assessed by applying First, Pseudo-first and second order kinetics on the photocatalytic degradation data for MO dye. The pronounced efficacy of the ternary composite compared to g-C₃N₄ alone confirmed its applicability for enhancing the photocatalytic potential under visible light. This study pioneers the investigation of the BiVO₄@HMT/g-C₃N₄ ternary composite's performance and novelty in the context of dye degradation. As a promising solution to the persistent challenge of dye-contaminated wastewater, the ternary composite opens avenues for more efficient, sustainable, and environmentally responsible wastewater treatment practices.

1. INTRODUCTION AND LITERATURE REVIEW

Water is considered as an abundant resource in the world, yet only 1% or less is safely available for human consumption (Mishra, 2023). One of the basic humanitarian aims is to have clean and affordable drinking water resources, which is still a major challenge of 21st century. Many previous and new challenges are in the way of the water supply chain. About 1.1 billion people around the world are deprived of clean and healthy drinking water (Helaimia, 2023). While water remains essential for both sustaining life and supporting livelihoods, it has emerged as an urgent global societal and geopolitical concern. This is underscored by the fact that approximately 800 million individuals across the globe lack reasonable access to clean drinking water, and a staggering 2.2 billion people do not have access to a safe water source. Consequently, the scarcity of freshwater resources has escalated to become the second most critical global issue, following closely behind the rapidly growing population dilemma (Helaimia, 2023). Should the challenge of freshwater scarcity persist unchecked, the global community is poised to fall significantly short of achieving water-related Sustainable Development Goals (SDGs). Projections indicate that by 2035, over 40% of the world's population will find themselves residing in regions grappling with severe water stress. This scenario will be marked by compromised ecosystems incapable of meeting the freshwater demands of their inhabitants. Notably, the impact will be most pronounced in developing nations, where a lack of access to clean water and compromised water quality will contribute to a staggering 80% of disease incidents (Shemer et al., 2023). Considering these concerns, urgent and coordinated efforts are imperative to address the impending freshwater crisis, as failure to do so will result in dire consequences for both human populations and the environment. Pakistan Council of Research in Water Resources (PCRWR) stated in May 2018, that there will be very little or no clean water in the country by 2025 (Nabi et al., 2019)

Different factors responsible for water-based issues include population growth, rapid industrialization and extensive urbanization that have constantly stressed water cycle. Climate change is a phenomenon that can amplify the uneven supply of water resource (Dinar et al., 2019). Various organic and inorganic pollutants are responsible for the contamination of water resource. Among them the emerging ones are endocrine disrupting chemicals, pesticides, synthetic dyes, and pharmaceutical compounds which enter the

environmental compartments (Kaczorowska et al., 2023). Surface water pollution is one of the emerging environmental issues resulting in addition of pollutants from both; point and non-point sources thus causing its quality deterioration. Among different groups, increasing proportion of dyes as effluent of industrial discharge is main cause water pollution and it has been proved as risk towards the health of water bodies for the past few decades (Zeghioud et al., 2020). Water is habitat for numerous life forms ranging from various types of planktons, protozoans, flora, and fauna. Dye effluent makes water unfit for various life forms by giving it colour and forming thin layer over water surface, hence reducing light penetration which affects processes of primary producers and oxygen suppliers through affecting photosynthetic activities of aquatic plants and algae, respectively (Waghchaure et al., 2022). Synthetic dyes find extensive applications across a range of industries including paper and pulp, plastics, food production, colour photography, leather goods, printing inks, textiles, pharmaceuticals, and cosmetics. While these sectors contribute significantly to the economic growth of developing countries, they also present significant environmental challenges. This is due to the routine discharge of substantial volumes of untreated waste, containing these synthetic dyes, into natural water sources used for drinking and other domestic purposes. The collective global output of industrial dyes, across various sectors, surpasses 9.9 million tons annually. Notably, the textile sector alone is responsible for disposing of approximately 2.8×10^3 tons of these dyes each year, often releasing them into local water bodies. The extensive production of synthetic dyes carries inherent risks to both human well-being and the environment (Waghchaure et al., 2022). Addressing these concerns, it is crucial to recognize that the large-scale production and utilization of such dyes can have far-reaching adverse effects, particularly in regions where they are dumped. Of particular concern is the potential harm to human health and the ecosystem. To mitigate the detrimental consequences associated with synthetic dyes, it becomes imperative to develop efficient and cost-effective treatment methodologies (Meurs, 2023).

1.1. Impact of Textile Industry on Water Resources

The textile sector holds significant importance as one of the world's largest export industries. In Asia, Pakistan ranks 8th in terms of textile product exports. However, within

conventional textile manufacturing, a notable environmental challenge arises as approximately 100 L of water are consumed for every 1 kg of textile material processed. This results in considerable water usage and subsequent waste generation. Notably, on a global scale, the discharge of industrial waste contributes around 0.28 million tons of textile dyes, further adding to environmental concerns (Arslan et al., 2023). The pollutants found in textile wastewater predominantly include organo-chlorines, dyes, and heavy metals. Among these, textile dyes are of particular concern due to their complex chemical structures. These dyes often have high molecular weights and low biodegradability, contributing to their persistence in the environment. Consequently, the direct release of untreated effluents containing these dyes into sewage systems introduces a range of harmful components, including acids, bases, and inorganic substances, into biological systems. This disruption in the normal biological degradation process ultimately results in increased capital costs for addressing these issues (Ingrassia et al., 2023). Addressing these complexities in the textile sector's waste management is crucial to mitigate the environmental impact of textile production. Developing effective strategies to treat and manage the effluents generated by textile manufacturing processes can help minimize the release of pollutants into the environment, leading to more sustainable industry practices. Textile industry is the backbone of Pakistan's economy and large several textile industries are situated in Karachi and Faisalabad. These industries discharge wastewater without any treatment draining through manmade channels. Wastewater treatment problem need to be addressed by both Government and researchers. Recycling of wastewater is need of the hour but presence of toxic organic compounds in wastewater is an obstacle to water recycling (Noreen & Younes, 2023).

1.2. Industrial dyes: An Overview

A dye functions as a substance utilized to infuse colour into various products or materials such as paper, leather, textiles, rubber, plastics, and cosmetics. These dyes are categorized as pigmented organic compounds with the primary purpose of colouring a wide spectrum of substrates, including textiles, paper, fur, waxes, greases, plastics, pharmaceuticals, hair, cosmetics, and leather items. This colouration process involves the creation of a chemical bond between the dye and the substrate. It's important to differentiate between dyes and

pigments; while dyes establish a chemical bond with the substrate, pigments lack this capability (Islam et al., 2023).

Typically, an aqueous solution of the dye is applied, and the attachment of the dye to the material is often augmented through the use of a mordant. The colouration of a compound is due to the presence of a chromophore, which exhibits an affinity for specific acidic or basic functional groups such as hydroxyl, sulfonic acid, amine, amide groups, and others. This inherent affinity is responsible for the vibrant colouration of the dye. The solubility of the dye in water can be attributed to the polar auxochrome group present, which interacts with oppositely charged groups on the fabric's surface. This interaction facilitates the attachment of the dye to the fabric, resulting in the desired colouration (Pratiwi et al., 2019). The interplay of these chemical properties underscores the fundamental mechanisms of dye-based colouration in various applications.

1.3. Historical use of Dyes

In the earliest epochs, the predominant utilization of dyes revolved around the employment of natural sources. Among these, indigo and alizarin stand out as two significant natural dyes harnessed during primitive times. Indigo dye, extracted from the leaves of the dyer's woad herb, held a pivotal role in early colouration processes. In those nascent stages, colours were derived from animal, vegetable, and mineral origins, often without undergoing any substantial processing (Ayele et al., 2021).

It wasn't until a serendipitous moment in 1856 that the trajectory of dyes took a transformative turn. This marked the fortuitous discovery of the first synthetic dye known as Mauve, by the hands of William Henry Perkin. The accidental creation of Mauveine led to a seismic shift in both the realm of artificial dyes and the broader field of chemistry itself. This momentous event set off an era of remarkable advancements in dye synthesis, laying the foundation for the vibrant world of synthetic dyes. Unlike their natural counterparts, synthetic dyes are intricate aromatic compounds synthesized through a range of complex chemical processes. These synthetic dyes offer an extensive palette of colours, far surpassing the limitations of their natural counterparts (Ayele et al., 2021). This marked

the beginning of a new era in the world of coloration and chemistry, forever altering the course of dye production and utilization.

1.4.Toxicity of Dyes

The global textile industry, while generating substantial revenue, approximately 1 trillion dollars, equivalent to 7% of total global exports, is also one of the most environmentally polluting sectors. Its significant use of fuel and chemicals, combined with the large-scale production and utilization of industrial dyes, contributes to water pollution on a large scale. This has raised serious concerns worldwide, prompting ongoing research in this domain. The environmental impacts of the textile business are extensive, including the release of particulate matter, dust, nitrogen and sulfur oxides, and volatile organic compounds into the atmosphere (Nipun, 2023). The discharge of effluent from the textile industry presents a considerable challenge due to its substantial volume and often unfavorable composition, frequently manifesting as a hazardous environmental concern. However, the consequences extend far beyond mere physical characteristics. The presence of textile colourants in water bodies not only tarnishes their visual appeal but also disrupts the natural flow of light, resulting in reduced photosynthetic activity and decreased levels of dissolved oxygen. This disruption has a profound impact on the entirety of aquatic life (Castillo-Suárez et al., 2023).

The effects of textile dyes on aquatic ecosystems are indeed alarming. These dyes carry inherent toxic, genotoxic, and carcinogenic properties, rendering them persistent ecological contaminants. Furthermore, their journey through the food chains leads to a phenomenon known as bio magnification. This intricate process results in the amplification of contamination levels as these dyes move up the trophic levels, accumulating in organisms that occupy higher positions in the food web. As a result, prey organisms, which occupy lower trophic levels, can bear an increasingly larger burden of contamination from textile dyes through their predators. This interconnected contamination amplification poses a significant threat to the overall health and stability of aquatic ecosystems. The intricate relationships within aquatic ecosystems underline the need for comprehensive strategies to mitigate the impact of textile dyes on water flora and fauna. By addressing both the immediate environmental challenges posed by textile dye effluents and the long-term

consequences of their persistence in ecosystems, we can work toward preserving the delicate balance of aquatic life while safeguarding human health and broader ecological integrity (Lekhak, 2023). It has been estimated that a substantial portion, ranging from 15% to 50% of azo dyes fail to effectively bond to fabric during the dyeing process. Consequently, these dyes are released into sewer water, which, notably, is frequently repurposed for irrigation in underdeveloped regions of the world. This practice, while seemingly pragmatic, can have significant repercussions. The toxicity associated with azo dyes stems from their chemical structure, particularly the presence of azo (-N=N-) groups. These groups can undergo transformation in aquatic environments, producing aromatic amines as byproducts. These aromatic amines are of concern due to their potential to induce toxicity and even genotoxicity. When azo dyes are used in textiles, they might remain unreacted and are subsequently released into water bodies during laundering or through other means. Once discharged, these azo dyes can be transformed into aromatic amines under the influence of various environmental factors like sunlight, temperature, and microbial activity (Vaiano & De Marco, 2023).

The deleterious impact of certain azo chemicals on microbiological populations is a significant concern. Azo dyes and their breakdown products can negatively affect the microbial communities present in soil and water, disrupting the ecological balance. Microorganisms play critical roles in maintaining soil fertility, water quality, and overall ecosystem health. Disrupting these microbial populations can have far-reaching consequences, affecting nutrient cycling, soil structure, and the overall health of the environment (George et al., 2023). The intricate interplay between azo dyes, their breakdown products, and the delicate ecosystems in which they reside underscores the importance of responsible dye usage and waste management practices. Mitigating the impact of these toxic compounds requires a comprehensive approach that considers both their immediate effects and long-term consequences. By doing so, we can strive to strike a balance between industrial practices and ecological preservation, particularly in regions where water resources are limited and essential for sustenance.

One study shed light on the toxic nature of degradation by-products originating from azo dyes (Ramireddy et al., 2023). These by-products were generated through an advanced

oxidation process that employed ozonolysis as a treatment method. The study's outcomes indicate that these degradation by-products exhibit a spectrum of harmful characteristics, encompassing carcinogenicity, immunotoxicity, and cytotoxicity. Moreover, their impact extends to essential factors such as androgen receptor and mitochondrial membrane potential. Predictions derived from test furnished valuable information by establishing LC50 and IGC50 values for a range of organisms. The EPI Suite, particularly through its Bioconcentration Factor/Bioaccumulation Factor (BCF/BAF) module, hinted at the significant potential for these degradation products to accumulate in organisms over time. The study underscores the urgency of implementing comprehensive strategies to mitigate the hazardous nature of these degradation by-products. It is consequently critical to employ treatment strategies that attempt to protect the environment's long-term viability for future generations by utilizing physical, chemical, and biological technologies, or a mix of these technologies. **Figure 1.1** provides the schematic illustration of dye pollution sources, sink and effects.

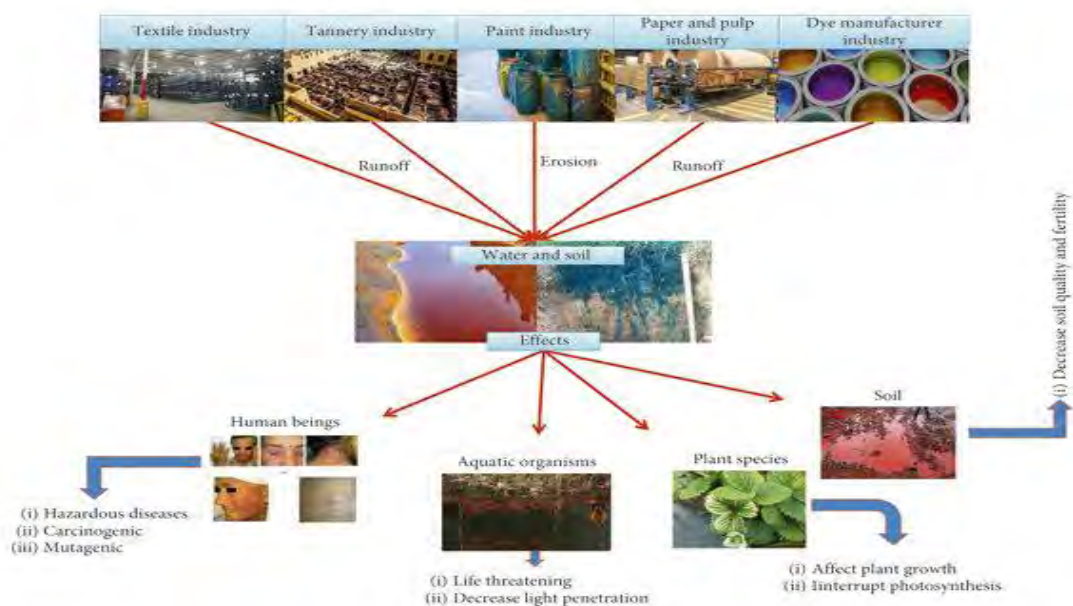


Figure 1.1: Schematic illustration of dye pollution sources, sink and effects. Source (Ayele et al., 2021)

1.5. Impacts of Dyes on Human Health

Various textile dyes, including methyl orange, malachite green, rhodamine B, methylene blue, and crystal violet, have widespread applications across industries like aquaculture, food, textiles, and medicine. However, their utilization poses considerable health risks to humans. Malachite green, while used as an antifungal agent, adversely affects the immune and reproductive systems, and exhibits cytotoxic, genotoxic, carcinogenic, and teratogenic properties (Tkaczyk et al., 2020). Similarly, rhodamine B, commonly employed in tracing water and various industries, demonstrates genotoxic, carcinogenic, and neurotoxic effects, causing harm when ingested, as well as skin, eye, and respiratory irritation (Hakami et al., 2021). Methylene blue, despite its medicinal uses, can lead to elevated blood pressure, myocardial depression, and other serious side effects, including tissue necrosis. Another category, the azo dyes, prevalent in textiles, leather, food, cosmetics, and more, poses mutagenic, carcinogenic, and genotoxic threats. Workers exposed to these dyes suffer from various cancers, and their usage has been linked to chromosomal aberrations (Sudarshan et al., 2022). In the case of specific dyes like metanil yellow, its common applications in colourants lead to gene expression alterations, carcinogenicity, and toxic effects like cyanosis and methemoglobinemia when ingested. Notably, methyl orange, used in the textile industry and as a pH indicator in laboratories, demonstrates toxic and mutagenic attributes, inducing both acute and chronic impacts on aquatic life. These findings emphasize the need for comprehensive understanding and regulations to minimize the detrimental health effects posed by the widespread use of these textile dyes (Sudarshan et al., 2022).

1.6. Distinguishing Between Dyes and Pigments

The fundamental difference between dyes and pigments lies in their behavior and application. A dye is essentially a coloured substance that exhibits a specific affinity for the material it is applied to, while a pigment operates by selectively absorbing certain wavelengths of light to alter the colour of reflected or transmitted light. These elements find use in a range of products, including plastics, paints, inks, textiles, and cosmetics, contributing to their chromatic characteristics (Pasdaran et al., 2023). The primary distinction between these two lies in their particle size, with pigments being notably larger than dyes. This size variance holds significance, as it influences stability. Dyes, due to their

fine particle size, are susceptible to degradation from ultraviolet (UV) radiation, unlike pigments that demonstrate a higher degree of stability in this regard. The application process further underscores their differentiation. Dyes, when dissolved in a liquid, are absorbed into the material, while pigments are suspended in the liquid, adhering to the surface of the substrate. Additionally, solubility in water serves as another discriminating factor; pigments are insoluble in water, while dyes exhibit solubility, allowing them to effectively dissolve in liquid mediums (Pasdaran et al., 2023).

1.7. Chemical Nature of Dyes

As the realm of dye chemistry advanced, scholars endeavoured to unravel the intricate relationship between chemical composition and the hues that emerge. This exploration led to the revelation that colours are not mere happenstance but are intricately tied to the underlying molecular structure. German chemists, in their quest to comprehend colour's essence, unearthed the profound significance of alternate double bonds. In these molecular arrangements, the presence of carbon, nitrogen, or oxygen alongside alternating double bonds formed the core of chromophores, the constituents responsible for absorbing and reflecting specific colours when subjected to visible light. Working in tandem with chromophores were auxochromes, functional groups that, while initially thought to be directly linked to dyeing capabilities, were later understood to independently influence the perceived colouration. This nuanced understanding was pivotal in the development of an overarching theory, culminating in the introduction of the term "chromogen" to denote the distinct combination of chromophore and auxochrome (Pasdaran et al., 2023).

1.8. Colour of Dyes

Within the fascinating realm of colouration, dyes and pigments harness the radiant energy of visible solar light to manifest their vibrant hues. Organic molecules, attuned to the subtle interplay of electromagnetic energy, that can absorb, and resonate with specific wavelengths, thereby unveiling a spectrum of colours. Notably, molecules endowed with numerous alternating double bonds emerge as colour bearers, owing to their propensity to absorb visible light. This absorption pattern, in turn, hinges on the molecule's degree of conjugation, influencing the wavelengths of absorbed light. The concept of energy gaps between molecular orbitals - the highest occupied molecular orbital (HOMO) and the

lowest unoccupied molecular orbital (LUMO) - comes to the front, playing a pivotal role in the energy exchange during the absorption process. Interestingly, molecular systems characterized by extensive conjugation necessitate higher energy sources such as ultraviolet (UV) radiation for electron excitation (Pasdaran et al., 2023). In contrast, dyes, characterized by narrower energy gaps, can effectively leverage lower energy sources like visible light to catalyse electron excitation. This intricate dance between molecular structure and absorbed energy culminates in the visible array of colours that captivate our senses.

$$AE(HOMO - LUMO) = hc/\lambda$$

The above formula quantifies the energy difference between a molecule's HOMO and its LUMO. This energy gap influences how the molecule interacts with light. Here, hc represents Planck's constant multiplied by the speed of light, and λ denotes the wavelength of light. In essence, this formula helps explain the energy transition that occurs when a molecule absorbs or emits light (Nagarajan et al., 2023).

1.9.Types of Dyes

1.9.1. Natural Dyes

In antiquity, natural sources were the primary reservoirs from which dyes were derived, showcasing an intimate connection between human creativity and the bounties of nature. A rich tapestry of colours was extracted from lichens, plants, trees, and even insects, offering a glimpse into the intricate craft of dyeing that stretches back over 4,000 years. Notably, the discovery of dyed fabrics within Egyptian tombs presents tangible evidence of the ancient origins of dyeing practices. Ancient civilizations, as evidenced by hieroglyphs, held a sophisticated understanding of the techniques required to extract and apply natural dyes. Despite these early endeavors, the extensive adoption of many natural dyes remained constrained due to their inherent instability and the intricate mix of compounds that composed them. Nevertheless, a select few natural dyes, among them alizarin and indigo, managed to emerge from the array of possibilities. Alizarin, for instance, obtains its vibrant red hue through an extraction process involving the roots of the madder plant (Bota & Indrie, 2021).

1.9.2. Mordants

An intriguing facet of the historical dyeing process is the strategic use of mordants, which served as the bridges between the dye molecules and the fabric substrates. Employing a range of metal salts, artisans enhanced the adhesion of dyes to fabrics and, intriguingly, unlocked the potential for creating a spectrum of colours through their interactions. Notably, in the annals of dyeing, the interaction between red, blue, and yellow dyes to produce diverse hues was a well-known practice. An interesting dichotomy emerges when considering cotton, which posed a unique challenge for dyeing due to its resistance to natural dyes. Here, mordants played a transformative role, enabling the application of colours to cotton through a process known as vatting or preparation. This innovative approach, involving inorganic salts as mordants, enabled the infusion of colour onto cotton textiles, transcending the limitations that were otherwise encountered (Bota & Indrie, 2021).

1.9.3. Synthetic Dye

The advent of synthetic dyes marked a seismic shift in the landscape of colouring agents, redefining the possibilities and potentialities of the industry. Pioneering this transformation was the serendipitous discovery of mauve by William H. Perkin in 1856, an event that triggered a cascade of change. This unprecedented innovation quickly reverberated throughout global markets, triggering the eclipse of natural dyes as synthetic counterparts began to dominate various sectors. The genesis of the synthetic dye industry can be traced back to the exploration of coal tar, a byproduct of coal processing. Recognizing its potential, chemists embarked on a journey to harness the organic compounds concealed within coal tar through the distillation process. This fateful convergence of science and industry set the stage for the rise of synthetic dyes, setting them apart from their natural predecessors and heralding a new era of vibrant and versatile colouration (Srivastava et al., 2021).

1.9.3.1. Classification of Synthetic Dyes

Synthetic dyes are commonly referred to as "coal-tar dyes" due to their predominant origin from coal tar, characterized by aromatic properties. In contrast, natural dyes are sourced from animals, plants, and minerals, without the involvement of chemical alterations. These

natural dyes encompass distinct categories, including vat dyes, substantive dyes, and mordant dyes. Conversely, synthetic dyes find extensive application in textile colouring, engaging in chemical bonding with fibre molecules to achieve their vivid effects. **Figure 1.2** represents classification of synthetic dyes on basis of solubility (Sharma et al., 2021).

Dyes can be systematically classified through two distinct approaches:

- **Constitution-Based Classification:** This approach categorizes dyes based on the specific functional groups responsible for their colouration. Notable examples comprise acridine dyes, nitroso dyes, indigoid dyes, azo dyes, triphenyl methane dyes, and nitro dyes.
- **Application-Based Classification:** Dyes are also categorized according to their suitability for specific applications, considering the nature of the dye and the fibres it interacts with. This classification encompasses acidic dyes, sulphur dyes, direct dyes, basic dyes, disperse dyes, azoic dyes, and vat dyes (Sharma et al., 2021).

Integral to comprehending dyes is their fundamental molecular structure, which includes crucial groups like chromophore, auxochrome, and matrix. The chromophore, acting as the active site, underpins the colour exhibited by the dye. Dyes encompass diverse classes contingent on their chromophores, including triphenylmethane, azo, diphenylmethane, and xanthene, each conveying distinct chemical arrangements. The nomenclature of textile dye colours is influenced by the molecular composition of their chromophore groups. Notably, the chromogenic chromophore, a collection of atoms within dye compounds, determines the hue, while an auxochrome chromophore, constituted by an additional assembly of atoms, enhances the chromogen's colour intensity. This systematic classification not only aids in comprehending the diverse spectrum of dyes but also underscores their intricate interactions with the materials they colour (Slama et al., 2021).

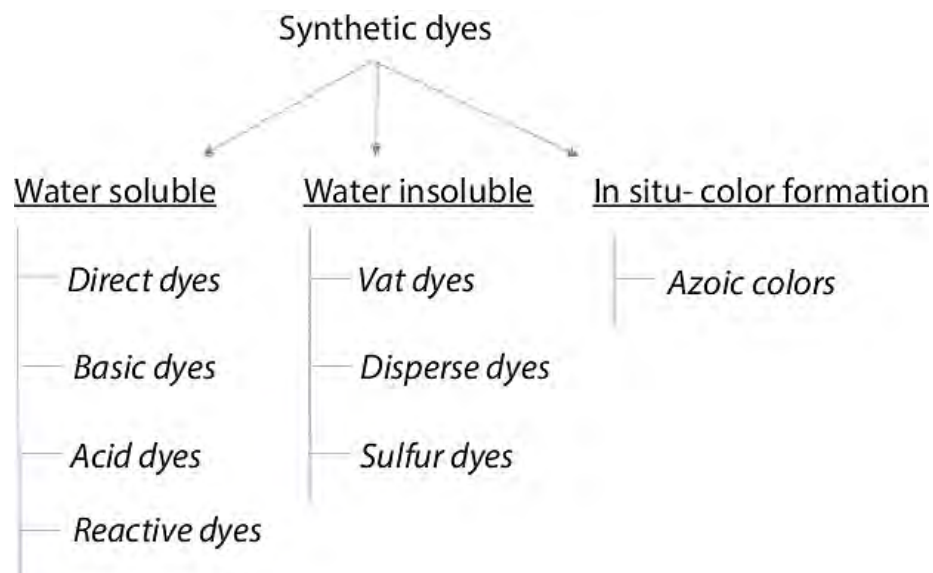


Figure 0.2: Classification of dyes based on their nature. Source: (Uddin & Rehman, 2018)

1.10. Characteristics of Azo Dyes

Azo dyes stand as one of the prevalent classes within synthetic dyes. Among their key constituents are auxochromes like NH, NR₂, and OH. Notably, azo dyes feature an aromatic group linked to the azo moiety, shaping their distinctive chromophore. These dyes find widespread application in treating textiles, leather products, and certain food items. A parallel chemical counterpart to azo dyes is the insoluble azo pigments. An intriguing facet of azo dyes is their sensitivity to solution pH, which can result in variations in conjugation of bonds and consequently induce shifts in colour hue. A classification criterion for azo dyes revolves around the number of azo groups present within the molecule, leading to distinctions like mono-azo, diazo, and tri-azole compounds (Iwuozor et al., 2021). Here, we delve into the attributes of a notable azo dye, Methyl Orange.

1.10.1. Methyl Orange (MO)

Methyl orange, ‘Dimethylaminoazobenzenesulfonate’ is a typical employed azo anionic dye. When dissolved in water, this organic dye displays a vivid orange colour and has a high colourability. As represented in **Figure 1.3**, azo dyes, like MO contain aromatic and -N=N- groups in their molecules. As discussed above, these groups are highly poisonous, detrimental, and carcinogenic to the environment and organisms.

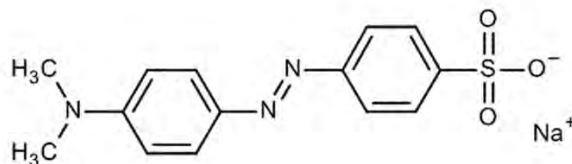


Figure 0.3: Chemical structure of Methyl Orange dye. Source: (Regraguy et al., 2022)

Methyl Orange serves as a pH indicator widely utilized in titration due to its distinct and evident colour transition across varying pH levels. In acidic conditions, MO manifests a red hue, while it transforms into yellow in basic environments. Its ability to exhibit a colour change at the pH of a moderately strong acid makes it particularly valuable in acid titrations. Unlike a universal indicator, MO presents a sharply defined endpoint without encompassing an extensive spectrum of colour transitions. While MO is recognized for its capacity to dye wool and silk, its colour tends to fade upon exposure to light or washing. Interestingly, MO is predominantly utilized as an indicator for acid-base titrations rather than primarily serving as a colouring agent. Its pH sensitivity ranges from 3.1 to 4.4. The shift in colour arises from variations in ion structure between acidic and basic media, each displaying specific chromophores (Yadav & Dasgupta, 2022). Refer to **Figure 1.4** for a visual representation of the structural alterations in MO as pH shifts.

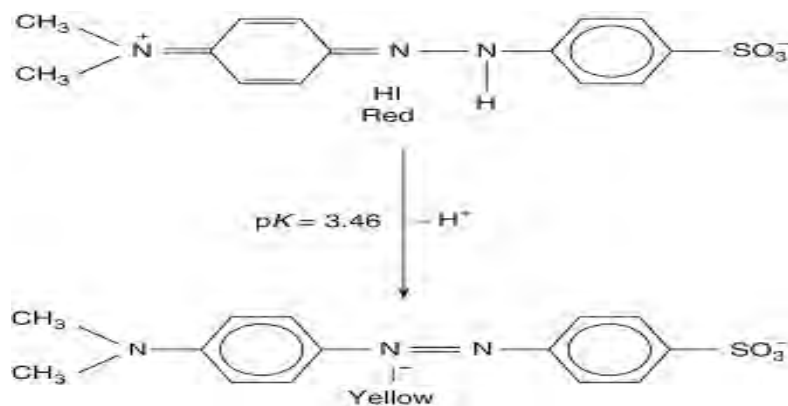


Figure 0.4: Effect of acidic and basic media on the Colour change of MO. Source: (Malviya et al., 2015).

1.11. Conventional Methods used for Treating Textile Effluent

In response to growing apprehensions about the health implications linked to colourants in wastewater discharge, there is a global drive to enhance colour removal methodologies. Numerous nations have enacted stringent environmental regulations mandating the pre-treatment and elimination of dyes from wastewater before their discharge into aquatic ecosystems. Addressing the efficient and proficient treatment of substantial volumes of dye-laden effluents has emerged as a significant challenge, as no singular system proves universally effective in degrading diverse dye compounds (Seow et al., 2016). A succinct exploration of wastewater treatment technologies is presented in **Figure 1.5**.

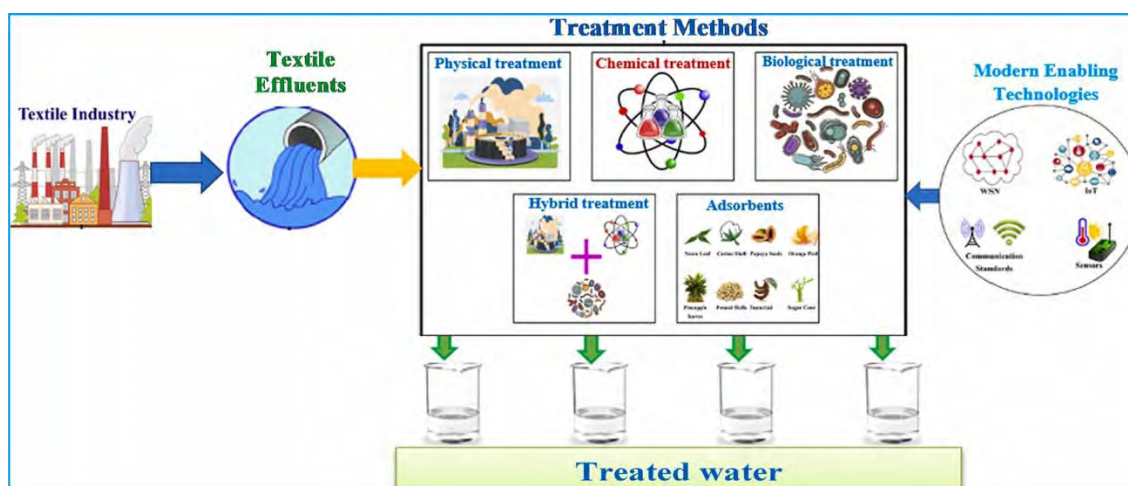


Figure 0.5: Schematic diagram of treatment methods for textile wastewater. Source (Azanaw et al., 2022)

1.11.1. Biological Methods

Biological approaches offer cost-effective and user-friendly techniques for dye degradation and de-colourization. These methods encompass anaerobic, aerobic, or hybrid processes that integrate both conditions. In the context of aerobic treatment, microorganisms such as bacteria and fungi have garnered significant attention for their potential to remediate coloured wastewaters. Within this milieu, bacteria release enzymes that facilitate the degradation of organic compounds present in dye-contaminated wastewater. However, the effectiveness of this approach varies, as certain dyes prove detrimental to microorganisms, thereby reducing the efficacy of biological degradation (Selvaraj et al., 2021).

For dyes that exhibit resilience under aerobic conditions, the anaerobic method emerges as a solution. Anaerobic treatment stands out as a widely employed technique for effective dye degradation. This method holds the capacity to efficiently decolorize dyes while maintaining cost efficiency. The process leverages sulfate reduction to retain essential metals, eliminates biological oxygen demand (BOD), and capitalizes on elevated wastewater temperatures to enhance anaerobic dye degradation. Nevertheless, drawbacks include incomplete degradation of dyes and other organic compounds, as well as the generation of sulfite due to compromised nutrient removal, like nitrogen and sulfur (Selvaraj et al., 2021).

Furthermore, a combined aerobic-anaerobic approach has been proposed to bolster the decolonization of textile effluents. This synergistic strategy capitalizes on the interactions among various microorganisms, facilitating complete de-colorization of dye-contaminated effluents. While this methodology proves cost-effective and suitable for various dye types, challenges arise in the form of aromatic amine production, incomplete degradation, substantial operational and capital expenses, and the spatial demands, rendering it less suitable for the treatment of extensive wastewater volumes (Selvaraj et al., 2021).

1.11.2. Filtration Technology

Filtration techniques play a pivotal role in wastewater treatment, constituting a crucial physical process. Various filtration methods, including reverse osmosis, microfiltration, ultrafiltration, and nanofiltration, are employed to address the challenges posed by coloured water. Tailored membranes, specifically designed to suit the requirements of each filtration technique, are deployed for this purpose. Despite its utility, membrane filtration faces limitations in wastewater treatment, primarily attributed to rapid membrane clogging and fouling, substantial energy demands, high initial costs, and the need for membrane protection, rendering it an economically unviable option for countries such as Pakistan (Selvaraj et al., 2021).

Reverse osmosis stands out as an effective method in this domain. This process involves the passage of water against the concentration gradient through a semipermeable membrane under pressure. While reverse osmosis excels in blocking salts, its scope is

limited when it comes to removing small organic molecules with molecular weights below 200, as well as weak acids and bases that lack ionization. This method proves particularly efficient for recycling by eliminating inorganics, colour, and salt from both seawater and wastewater. The water obtained through reverse osmosis attains an exceptional level of purity, reaching close to 100% (Selvaraj et al., 2021).

1.11.3. Coagulation/Flocculation

Employing a blend of physical and chemical mechanisms, this method emerges as a potent treatment approach for eliminating dyes associated with textiles, organic compounds, and heavy metals from wastewater streams. The procedure hinges on the deployment of coagulants, such as aluminum (Al), calcium (Ca), or ferric ions (Fe^{3+}), to facilitate its efficacy. In certain cases, a dual coagulant strategy is adopted to enhance the treatment process. While this technique generally proves economically feasible, apart from the chemical costs, a significant limitation lies in the generation of concentrated toxic sludge as an end product. Moreover, the treatment's effectiveness is contingent upon factors such as pH levels, contributing to the intricacies of its implementation (Bal & Thakur, 2022).

1.11.4. Oxidation

Several oxidation processes play a pivotal role in either partially or completely oxidizing the textile dyes found in wastewater discharged from the textile industry. Ozone (O_3), chlorine (Cl), hydrogen peroxide (H_2O_2), UV/ TiO_2 , potassium permanganate (KMnO_4), and Fenton's reagent are notable contenders in this realm. These methods leverage the reactivity of chemicals boasting high oxidation potential, generating hydroxide radicals ($\text{OH}\cdot$) that possess the capability to catalyze the oxidation of specific compounds, thereby effectively decolorizing dyes. Nonetheless, these techniques aren't without their drawbacks. Chlorine, while effective, gives rise to unintended side reactions that yield aromatic amines, and in cases of metal complex dyes, metals can leach out, potentially compromising metal-based utensils (Vaiano & De Marco, 2023). Hydrogen peroxide (H_2O_2), renowned for its robust oxidative and bleaching properties in applications like paper bleaching, is pH-sensitive, leading to secondary waste production. Fenton's reagent, a concoction of ferric catalyst and H_2O_2 , is employed for dye wastewater oxidation. However, its efficacy hinges on a limited pH range (<3.5), and its application is hampered

by extended reaction times and the byproduct of sludge. Ozonation, involving the utilization of ozone generated from molecular oxygen, also contributes to dye removal within a specific range. Regrettably, the high cost associated with this process poses a considerable barrier. Electrochemical approaches, employing water-insoluble anodes like iron (Fe), polymers, and boron-doped diamond electrodes, demonstrate efficiency in addressing both soluble and insoluble dyes. Yet, the method's significant downsides encompass sludge generation, the formation of chlorinated organics, and substantial energy consumption (Isaev et al., 2023).

1.12. Approaches for Mineralization of MO

An overarching challenge lies in the inadequate management of municipal and industrial wastewater, leading to non-compliance with discharge standards and subsequently affecting both water quality and soil fertility. This scenario underscores the pressing need for effective, straightforward, and economically feasible solutions to mitigate the impact of these pollutants on the environment (Wang et al., 2022a). Given MO's limited biodegradability, targeted interventions are essential for its removal. A range of approaches, including chemical, biological, and physical methods, have been explored. Notably, advanced oxidation processes (AOPs) have garnered attention for their potential in addressing this issue. AOPs offer the advantage of achieving near-complete degradation of soluble organic contaminants in fluids and soils, owing to the generation of potent hydroxyl radicals that effectively transform pollutants into harmless substances like carbon dioxide and water. Rapid and efficient AOPs hold promise as a viable solution for wastewater treatment, characterized by their ability to minimize solid waste production (Wang et al., 2022b).

1.12.1. Heterogeneous Photocatalysis

In the realm of AOPs, semiconductor photocatalysis emerges as a promising technique for thoroughly breaking down organic contaminants and harmful dyes. Photocatalysis accelerates light-triggered chemical reactions in the presence of a catalyst known as a photocatalyst. In this process, a substrate with adsorption capabilities interacts with light, leading to chemical transformations (H. Wang et al., 2022). The potential of photocatalysis extends across diverse scientific disciplines, as highlighted in **Figure 1.6**.

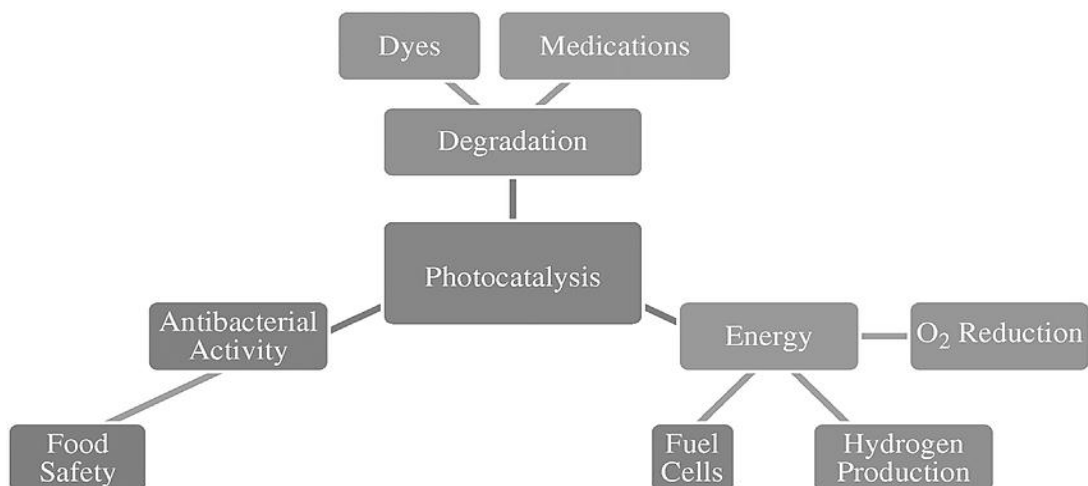


Figure 0.6: Prospective applications of photocatalysis. Source: (Tatarchuk et al., 2018).

In heterogeneous catalysis, the catalyst used exists in a different phase compared to the reactant substance. Photocatalysts, such as transition metal oxides and semiconductors like BiVO_4 , TiO_2 , WO_3 , CdS , ZnO , and ZnS , play a pivotal role in this process. These substances possess distinct properties that enable them to initiate photocatalysis effectively. While metals exhibit a continuous range of electronic states, semiconductors possess an energy zone devoid of electrons. This absence of energy levels between electrons and holes makes electron-hole recombination challenging after photoexcitation (Liu et al., 2022).

The term "band gap" signifies the empty region situated between the filled valence band (VB) and the empty conduction band (CB) within a semiconductor. When a photon carrying energy equivalent to or greater than the semiconductor's band gap is absorbed, it triggers the stimulation of an electron from the valence band to the conduction band, leaving behind a positive hole. This generated electron-hole pair is termed an "exciton." Despite this, excited electrons and holes may recombine due to the subsequent emission of a photon. An ineffective catalyst fails to effectively prevent this recombination of charges, which can limit the efficiency of the photocatalytic process (Younis & Kim, 2020).

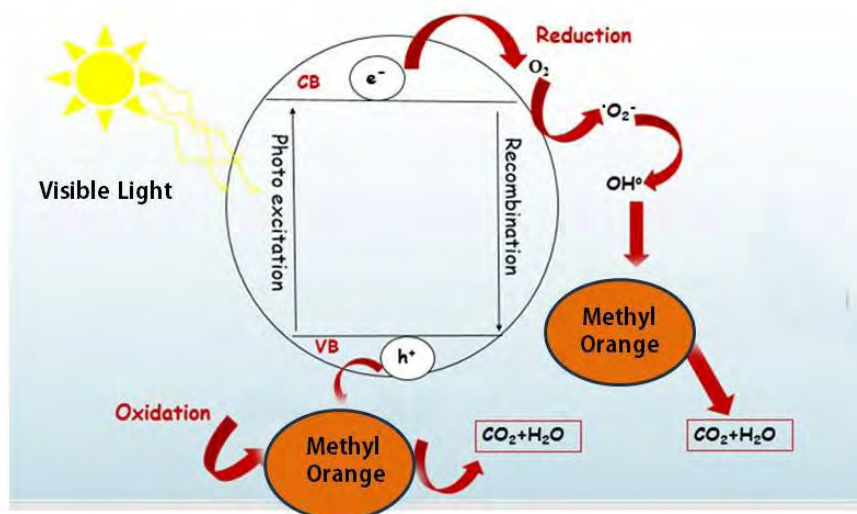


Figure 0.7: Schematic diagram of heterogeneous photo catalysis.

1.13. Nanoparticles and Photocatalytic Properties

Nanotechnology involves the exploration and advancement of objects on a scale akin to atoms and molecules. The fundamental unit of measurement at this level is the nanometer, which corresponds to one billionth of a meter. Nanotechnology holds promise for innovative solutions to challenges encountered by developing nations, particularly in domains like food security, environment, health, and sanitation. By employing nanoscale materials, encapsulation systems can be devised to protect and gradually release contained medications, which could prove invaluable in regions with limited storage and distribution networks, as well as for individuals requiring complex treatment regimens that entail substantial travel distances (Bhattacharjee et al., 2022). One significant application is in water filtration, where nanoscale-structured filters could yield more cost-effective, durable, and easily maintainable systems. Nanotechnology has generated an array of materials at the nanoscale, with nanoparticles (NPs) being particles with a size as small as 100 nanometers. NPs exhibit distinctive physical and chemical attributes compared to their larger counterparts due to the altered behavior of substances on the atomic scale. This shift occurs as the surface-to-volume ratio expands, leading to surface atoms influencing the material's properties. NPs possess an unusually significant surface-to-volume ratio due to their diminutive size, allowing them to confine electrons and exhibit quantum effects. These

unique properties, if harnessed effectively, hold considerable potential for diverse applications (Bhattacharjee et al., 2022).

1.13.1. Bismuth Vanadate Nano-powders

Bismuth vanadate (BiVO_4) has gained significant prominence as a visible light active photocatalyst, largely attributed to its array of commendable attributes. Its distinct characteristics, including its status as non-toxic photocatalyst, coupled with its remarkable chemical, electrical, and photonic properties, underscore its potential for versatile applications. Among its crystalline forms, specifically the 'tetragonal zircon,' 'tetragonal scheelite,' and 'monoclinic scheelite' structures, the monoclinic scheelite configuration emerges as particularly noteworthy. This structure stands out due to its heightened photocatalytic activity, primarily attributable to its remarkably low band gap energy of 2.4 eV. However, the significance of BiVO_4 's photoactivity extends beyond its structural disposition. Its electronic structure acts synergistically with its crystal morphology, facilitating efficient energy absorption within the visible light spectrum (Zhang & Li, 2020). The intricate electronic dance within BiVO_4 's valence band, characterized by hybridized O 2p and 6s orbitals, plays a pivotal role. This structural configuration enables the 'photoexcited electron' to effortlessly traverse the small distance to the vanadium's 3d orbital, resulting in the provision of diminutive band gap energy. Despite these commendable traits, BiVO_4 does encounter occasional hurdles, including the recombination of e^-/h^+ pairs, leading to instances of reduced activity. To mitigate this concern and bolster its photocatalytic prowess, several strategic maneuvers are at disposal. One effective avenue involves structural manipulation, achieved through the creation of heterojunctions with catalysts featuring either larger or smaller band gaps, supplemented by doping or co-catalyst integration (Guo et al., 2022).

The synthesis of BiVO_4 , propelled by diverse techniques, has captivated the interest of researchers within the field. These methodologies encompass a spectrum of approaches, encompassing microwave-assisted, hydrothermal, co-precipitation, solution-combustion, and sol-gel methods. These techniques frequently employ starting materials such as bismuth (III) nitrate pentahydrate ($\text{Bi}(\text{NO}_3)_3 \cdot 5\text{H}_2\text{O}$), Ammonium Vanadate (NH_4VO_3), or Sodium Vanadate (NaVO_3). A salient aspect of our study pertains to the potential of

BiVO₄-based nanostructures. These structures exhibit a pronounced capability to address the degradation challenges posed by persistent organic pollutants, including methyl orange (MO) dye. This underscores BiVO₄'s promising role in addressing the intricate conundrums associated with environmental contaminant removal and remediation (Rajaiitha et al., 2022).

The interaction between dye molecules and photocatalyst surfaces is significantly influenced by the charges present in these molecules, leading researchers to target specific ionic forms that enhance adsorption capacity. For example, successful adsorption of Methyl Blue (MB) onto semiconductor surfaces has been achieved through electrostatic interactions, driven by the zeta potential. The positively charged cationic form of MB exhibits densely packed adsorption on the negatively charged photocatalyst surface. Similarly, the creation of a Bismuth Vanadate/Titanium Dioxide (BVO/TiO₂) nanocrystalline heterostructure via a modified sol-gel and hydrothermal approach has resulted in efficient photocatalytic performance (Lotfi et al., 2022). Another notable study introduces a novel composite of Bismuth Vanadate combined with carbon spheres (BVO-0.18 C) for enhanced adsorption and photocatalysis. The pH-dependent behavior of this composite reveals its highest photocatalytic activity and adsorption efficiency for Methyl Blue (MB) and Rhodamine B (RhB). Electrostatic attraction between the negatively charged dyes (MB and RhB) and the positively charged BVO-0.18C composite contributes to this outcome. Moreover, a CdS/BVO heterostructure demonstrates that an optimal pH of 5 facilitates Rhodamine B (RhB) photodegradation due to electrostatic interactions. Acidic conditions hinder photodegradation efficiency, while alkaline solutions enhance adsorption (Zou et al., 2019). Further exploration includes the adsorption behavior of MO on conducting Polyaniline–BVO nanocomposites. Incorporating BVO within the Polyaniline matrix, coupled with the electrostatic attractive force between the anionic MO and the positively charged Polyaniline backbone, contributes to the remarkable adsorption capacity. Lastly, the efficacy of a p–n heterojunction Ce₂O₃/BVO embedded in reduced graphene oxide for the adsorption and degradation of MO under visible light has been investigated. The favorable adsorption ability between anionic MO molecules and the catalyst surface, particularly in an acidic environment, leads to the superior photocatalytic performance of this heterojunction (Onwudiwe et al., 2021).

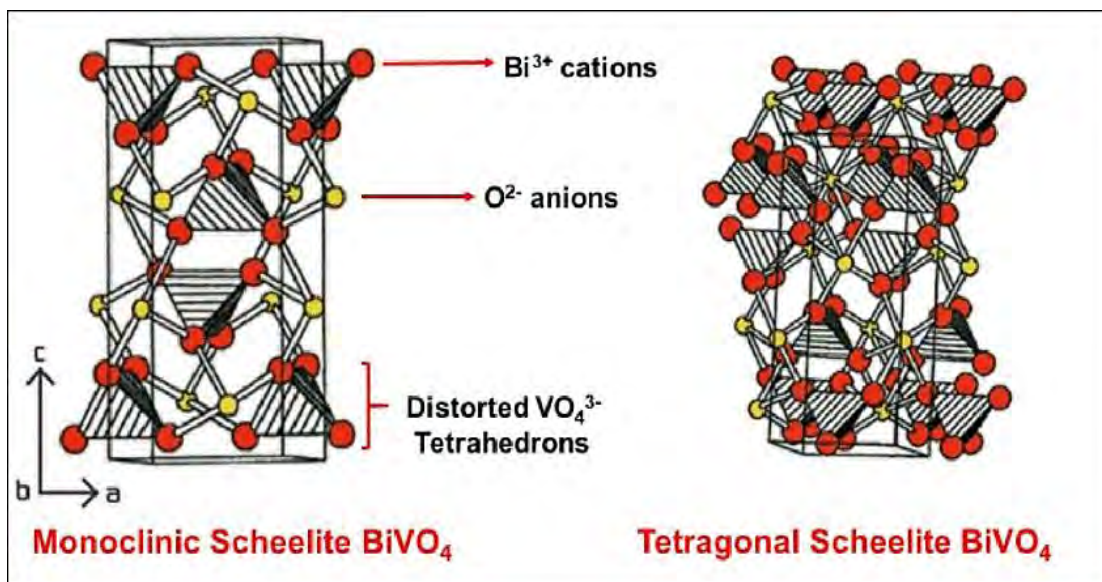


Figure 0.8: Crystalline phases of BiVO_4 . Source: (Anusuyadevi., 2018)

1.13.2. Hydrogen Peroxide Modified Titania Powders

Photocatalysis employing titanium dioxide (TiO_2) represents the fusion of photochemistry and catalysis. Despite its larger band gap primarily absorbing solar energy in the UV region, TiO_2 's role as a singular photocatalyst has been somewhat subdued by the advent of visible light-active catalysts. Nevertheless, its advantages including stability, biocompatibility, affordability, and advantageous band edge positions continue to render it indispensable. Exploration into the inhibition of bacterial growth employing unadulterated, doped, and heterojunctioned TiO_2 has yielded valuable insights. Enhancing the degradation efficiency of pollutants has spurred interest in peroxide activation as a promising technique. In this approach, metallic catalysts like Palladium (Pd) and Gold (Au) are integrated or doped into TiO_2 due to their remarkable capacity for generating H_2O_2 . Another effective method involves direct introduction of H_2O_2 into the photocatalytic system, resulting in the formation of hydroxyl radicals ($\cdot\text{OH}$) and thus facilitating efficient pollutant degradation. For instance, researchers found that optimal H_2O_2 dosages yield maximum degradation efficiency for Congo red dye. The interaction between H_2O_2 and TiO_2 leads to the creation of a titanium peroxide complex, $\text{TiO}_2\text{-H}_2\text{O}_2$, on the surface of

TiO₂. This complex triggers an electron transfer from the surface complex to the conduction band of TiO₂. Consequently, the photoabsorption of TiO₂ is shifted to the visible light region, broadening its photoactivity range and enabling effective degradation of organic dyes (Idris et al., 2022). Among the domain of 'non-metallic modifications,' the introduction of hydrogen peroxide (H₂O₂) has surfaced as a potent mechanism to reshape the crystal lattice of Titania, thereby enabling light absorption in the visible spectrum. This transformative alteration has demonstrated notable efficacy in the degradation of diverse organic compounds (Arun et al., 2022). Though both TiO₂ and H₂O₂ independently remain limited in their capacity to absorb visible light, their harmonious fusion yields remarkable results. Upon integration, the -OOH group of H₂O₂ takes the place of the -OH group on the surface of titania particles, giving rise to hydrogen peroxide-modified titania (HMT). This modification imparts a distinctive yellowish hue attributed to the formation of 'peroxo-complexes.' Remarkably, this alteration induces a shift in titania's absorption spectrum from the UV to the visible spectrum through a characteristic red shift. Empirical evidence corroborates the augmented degradation performance of organic compounds, encompassing substances like naproxen, linuron, humic acids, and dyes, upon exposure to HMT under visible light irradiation. Thus, the dynamic interplay of TiO₂ and H₂O₂ serves as a promising avenue to harness visible light for enhanced photocatalytic remediation (Rashid et al., 2022).

1.13.3. Graphitic Carbon Nitride (g-C₃N₄)

g-C₃N₄ is a polymeric material containing Carbon, Nitrogen, and some impurity Hydrogen, attached by tri-s-triazine based configuration. It can be obtained from carbonaceous materials by replacing carbon atoms with nitrogen (Zhu et al. 2014). This two-dimensional polymer tends to form a p-conjugated planar sheet because of presence of aromatic heptazine unit (C₆N₇) and van der Waals force is responsible for connection between the interlayers; explicitly like that of graphite (Tan et al. 2015). In contrast to majority of other carbonaceous materials, presence of N and H atoms within g-C₃N₄ structure provides basic functional groups, motifs for Hydrogen bonding and electron rich surface properties which are necessary for catalysis. The abundant functional groups for example -NH₂, -NH groups on the surface of carbon nitride nanosheets provide vast reactive sites for adsorbing

reactant molecules (Chen et al., 2016). Therefore, it is assumed that g-C₃N₄ could possibly replace carbon in material applications. The g-C₃N₄ has good chemical stability, multiple defects, tunable electrical structure and thermally stability up to 600 °C (Tan et al. 2015). The extremely well-ordered heptazine (C₆N₇) units of g-C₃N₄ allow simple stacking of nanosheets through a π - π conjugate interaction and/or hydrophobic effect. Hence, it is expected that aromatic contaminants may adsorb on the π region of g-C₃N₄ plane (Fu et al., 2017).

Graphitic carbon nitride has emerged as an efficient catalyst, for breaking down pollutants like methyl orange dye. Its unique electronic and structural properties make it an excellent candidate for applications in photocatalysis. When exposed to light g-C₃N₄ can generate pairs of electrons and holes which are then used to facilitate reactions, including the degradation of organic compounds. In the context of methyl orange dye, g-C₃N₄ demonstrates impressive performance. Its adjustable bandgap allows it to efficiently absorb light in the spectrum ensuring utilization of solar energy. This energy is utilized to initiate processes that break down the dye molecules into less harmful substances. The large surface area and numerous active sites of g C₃N₄ further enhance its activity enabling a level of dye adsorption and reaction kinetics (Guo et al., 2017). Moreover, owing to its good chemical stability and facile fabrication methods and inherent stability enables its regeneration and allow it to be reused, thus minimizing the need for catalyst consumption, and reducing waste generation, thereby, contributing to the overall sustainability of the photocatalytic process (Xi-Jun et al., 2022).

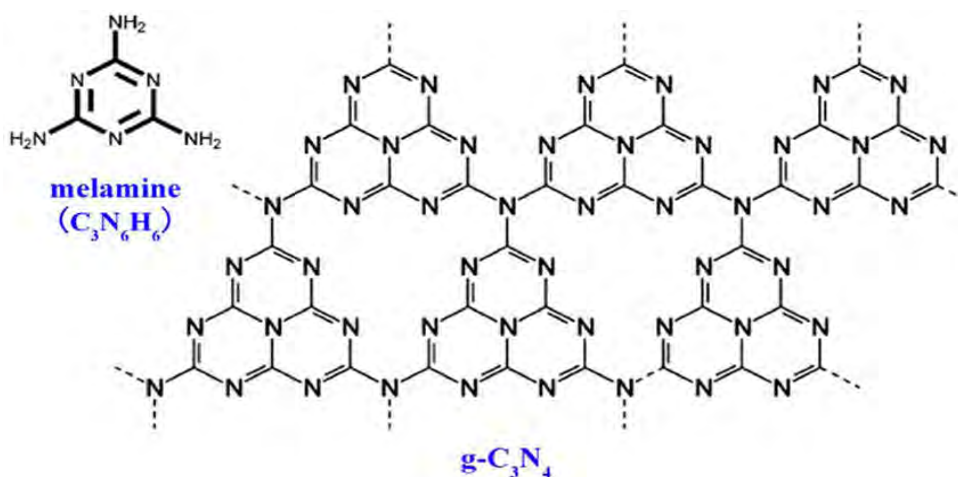


Figure 0.9: Structure of melamine and graphitic carbon nitride. Sources (Zhang et al., 2013)

1.14. Problem Statement

The escalating textile industries have exacerbated the release of dye wastewater, which includes hazardous compounds like methyl orange, into our water systems. Traditional treatment methods often result in the generation of numerous chemical agents and polymer electrolytes, leading to the creation of toxic sludge. This not only poses threats to aquatic ecosystems but also poses health risks to humans. Considering the limitations of conventional approaches there is a compelling need for innovative solutions such as advance oxidation through photocatalysis. However, further research in this area is crucial to develop and optimize novel photocatalysts that can efficiently degrade toxic dyes like methyl orange, paving the way for a more sustainable and effective approaches to wastewater treatment.

1.15. Aims and Objectives

1. Synthesis and characterization of g-C₃N₄ decorated with BiVO₄ and HMT ternary nanocomposite as a novel and effective visible light active photocatalyst.
2. Investigation of the photocatalytic degradation efficiency of pristine ternary nanocomposite compared to its pristine and binary components for removal of methyl orange dye from aqueous solutions under various experimental conditions (pH, catalyst dose, dye concentration)
3. Determination of the reaction kinetics of the photocatalytic process.

1.16. Significance of the study

Amidst the challenges posed by rapid population growth and the subsequent discharge of hazardous dye wastewater, particularly the detrimental methyl orange, the traditional methods of treatment are showing their limitations. These conventional techniques often result in the production of harmful byproducts and sludge, posing threats to both aquatic ecosystems and human health. Recognizing the inadequacies of these approaches there arises a critical need for innovative solutions. This study comes forth as a response to these challenges by exploring a novel approach to tackle the degradation of methyl orange. By investigating the photocatalytic degradation efficiency of a unique combination of g-C₃N₄ decorated with BiVO₄ and HMT, this research introduces a promising avenue for effective

dye removal from aqueous solutions. This approach capitalizes on the synergistic effects of different components, each contributing to the enhancement of the photocatalytic degradation process. Furthermore, the study aims to comprehensively assess the factors that influence the photocatalytic degradation efficiency of methyl orange under varying experimental conditions such as pH, catalyst dose, and dye concentration. By delving into the individual contributions and collective impacts of $g\text{-C}_3\text{N}_4$, HMT, and BiVO_4 , the research not only offers insights into the intricate mechanics of the process but also paves the way for the optimization of these components for enhanced dye removal.

2. METHODOLOGY

2.1. Materials

Materials used in this research included glassware such as Erlenmeyer flasks, beakers, test tubes, measuring cylinders and petri plates were made of Pyrex™, Borosilicate provided by Krishna and Normax companies. Other materials were amber glass bottles, Whatman filter paper No. 41 and 42, plastic test tube racks, magnetic stirring bars, syringe filters, Diamond aluminum foil, falcon tubes. The chemicals used in the preparation of methyl orange solution and photocatalysts were purchased from Sigma Aldrich, VWR and DAEJUNG. All the chemicals were of analytical grade and used without further purification.

2.2. Instruments

Instruments used for the current research were weighing balance (ATY224 Shimadzu), hot plate (VELP® Scientifica), pH meter (Adwa), Muffle Furnace (Ney® VULCAN), Photocatalytic chamber (Luzchem; LZC-4V), Drying Oven, Ultrasonic Bath Sonicator (Greatsonic GS-DS230), (XRD, Bruker AXS- D8, Germany) using Cu-K α ($\lambda = 1.5406$ nm) as source of radiation and secondary monochromator in the range 2θ from 10 to 80°, EDS were performed using Omicron system (Al K α 1486.7 eV X-ray source operated at 15 KeV), Scanning Electron Microscope (SEM) (Hitachi S 4800) at an operating voltage of 25 kV, and Transmission Electron Microscopy (TEM) were implemented on a JEOL (JEM-2100) electron microscope operating at the voltage of 20 kV.

2.3. Experimental Procedures

2.3.1. Preparation of Photocatalysts

The selected photocatalysts, BiVO₄, HMT, and g-C₃N₄ were prepared according to methods given in literature. BiVO₄ was prepared by using sol-gel method (Pookmanee et al., 2013) while HMT was prepared by soaking and microwave treatment method (Kang, 2017) and g-C₃N₄ was prepared by one step heating method (Liu et al., 2018).

2.3.2. Synthesis of BiVO₄

To synthesize the $g\text{-C}_3\text{N}_4$ powder the sol-gel method was adopted, synthesis scheme for 1g of powder is given in flow diagram (**Figure 2.1**). The starting precursors for this synthesis were Bismuth nitrate ($\text{Bi}(\text{NO}_3)_3 \cdot 5\text{H}_2\text{O}$) and ammonium vanadate (NH_4VO_3), added in stoichiometric amounts. ($\text{Bi}(\text{NO}_3)_3 \cdot 5\text{H}_2\text{O}$) and (NH_4VO_3) were dissolved in stoichiometric quantities of 4M HNO_3 and 4M NH_4OH named as solution A and B. After individual mixing for 30min in the solvents, solution A was mixed in solution B under continuous stirring which created yellow colour followed by the addition of ethanol. The obtained slurry was heated at 70°C for 1h, yellow sol was obtained. Sol was converted in yellow gel after the addition of 1M acetic acid and deionized water same in quantity as of solvents. The gel dried in drying oven at 100°C , until its moisture content vanished. After drying the obtained material was ground into fine powder using pestle and mortar followed by its calcination at 600°C for 2h. The formation of BiVO_4 powder is shown in **Figure 2.1**.

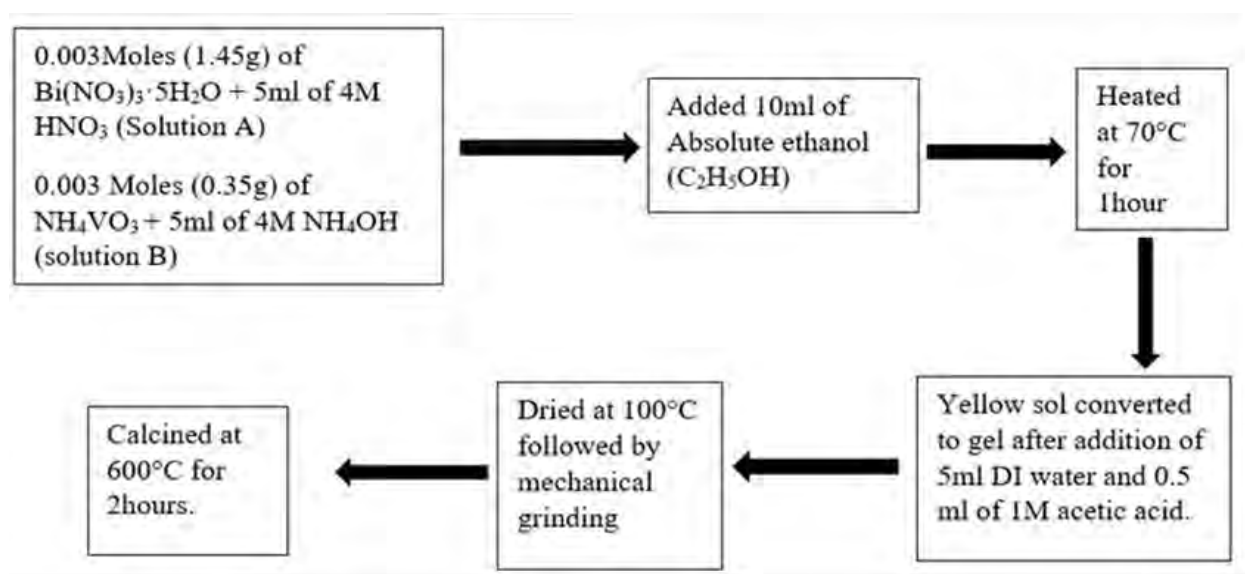


Figure 2.1: Scheme for synthesis of BiVO_4

2.3.3. Synthesis of Hydrogen Peroxide Modified Titania

HMT was prepared by simple soaking and microwave heating method where Degussa P-25 was soaked and stirred for 1 h in 3% solution of H_2O_2 followed by filtration and drying at low temperature. For synthesis of 1 g of HMT about 1.5 g of TiO_2 (Degussa P-25) was added in beaker with the addition of 30 mL of 3% H_2O_2 . The obtained yellow suspension was stirred for 1 h, filtered and dried at 60°C in drying oven until its moisture was

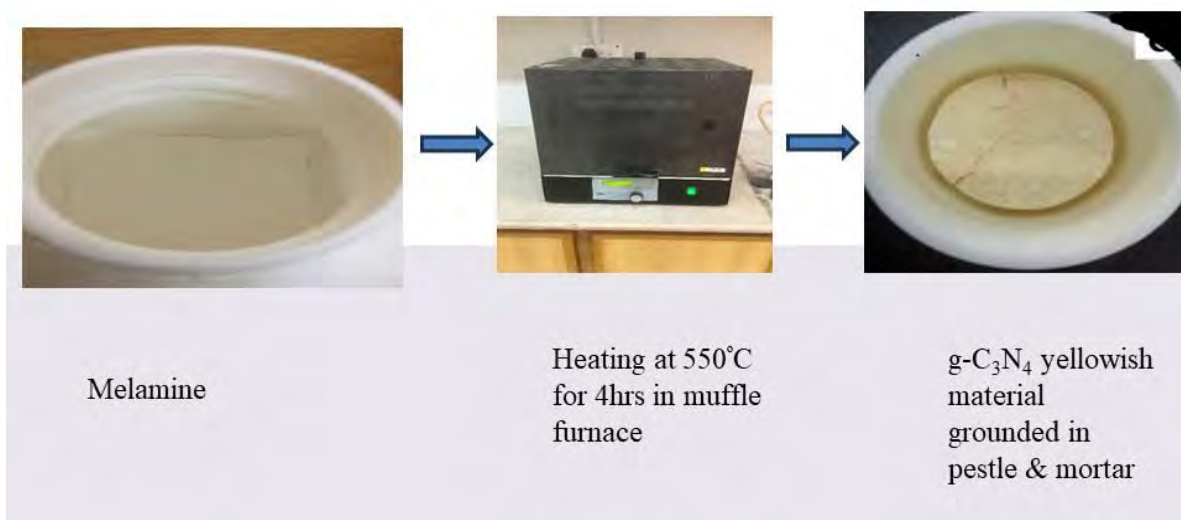
evaporated. Dried material had yellow colour and grounded into fine powder using pestle and mortar (**Figure 2.2**).



Figure 2.2 : Flow diagram of synthesis of HMT

2.3.4. Synthesis of Graphitic Carbon Nitride

To prepare graphitic carbon nitride ($g\text{-C}_3\text{N}_4$) direct heating of melamine was done, in the semi closed system to prevent sublimation. 20 g of melamine powder was put into an alumina crucible with a cover and then heated at $550\text{ }^\circ\text{C}$ in a muffle furnace for 2 h at ramping temperature $5\text{ }^\circ\text{C}/\text{min}$. Colour of powder was changed from white to yellow. After cooling, material was grounded into fine powder using pestle and mortar (**Figure 2.3**).



2.3.5. **Figure 2.3:** Flow chart of synthesis of graphitic carbon nitride ($g\text{-C}_3\text{N}_4$) **Preparation of Binary Composite**

For preparation of binary composite the HMT powder was modified using different fractions of BiVO_4 . For composite synthesis impregnation method was used where stoichiometric amounts of $(\text{Bi}(\text{NO}_3)_3 \cdot 5\text{H}_2\text{O})$ and (NH_4VO_3) and their respective solvents

dissolved for specific percentages of fractions (5%, 10%, 15%, 20%, and 25%). Followed by stirring of each solution for 30 min and addition of solution A and B, stirred for 15 min and addition of calculated amount of HMT as a base material in solution for each fraction, after vigorous stirring the ethanol was added and temperature maintained to 70 °C for 1 hour and the slurry was removed from stirring and hot plate after the addition of water and acetic acid, filtered dried and calcined at 600 °C.

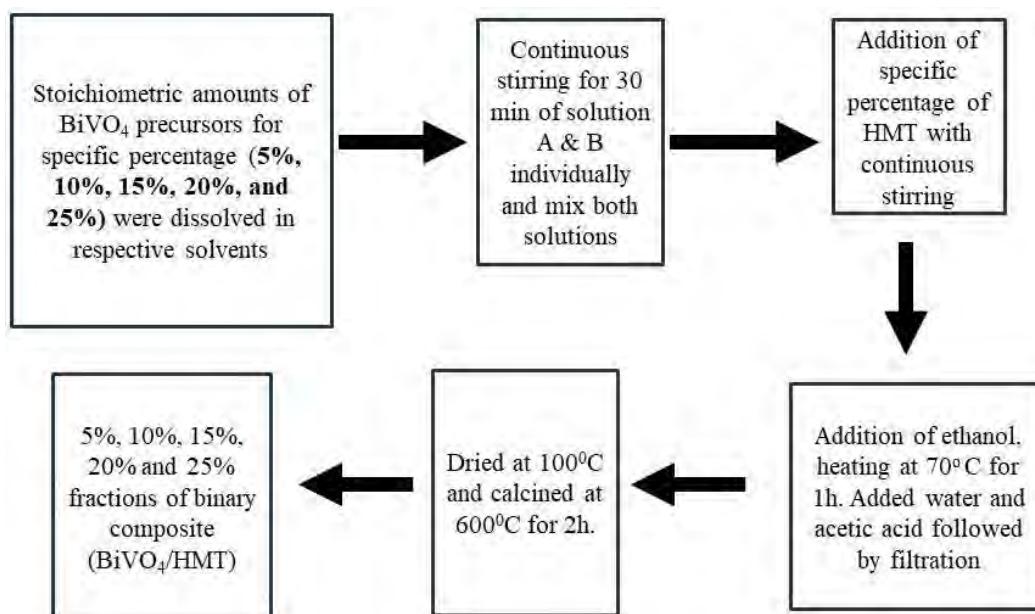


Figure 2.4: Synthesis of fractions of binary composite (BiVO₄/HMT)

2.3.6. Preparation of Ternary Composite

The ternary composite was prepared via ultrasonic dispersion and mixing method. The pre synthesized binary composite in section 2.3.5 was used along with graphitic carbon nitride powder prepared by the process discussed in section 2.3.6 to prepare various percentage fractions of ternary composite. A calculated amount of g-C₃N₄ was dissolved in 1:1 of water and ethanol solution and dispersed ultrasonically for 30 min, followed by addition of specific amount of binary composite (5%, 10%, 15%, 20%, and 25%), stirring vigorously for 30 min then filtered, oven dried at 70 °C for 1 h and calcined at 600 °C for 2 h. A dried material was then grounded to fine powder using pestle and mortar.

2.4. Photocatalytic Experiments

To test the photocatalytic degradation of methyl orange using prepared catalyst, photocatalytic experiments were performed in photocatalytic chamber (LZC-4V) decorated with visible cool white light lamps (14 x Sylvania F8T5/CW 8W lamps) collectively generating output of 20,000 Lux. To conduct the experiments, 100ml of methyl orange working solution was taken in a beaker from the stock solution. Afterwards, the photocatalyst was added and stirred in dark for the first 30 minutes. Following the initial period, the lights were switched ON. At regular intervals of 30 minutes, 3-4mL sample aliquots were taken from the solution using a 5mL syringe while each sample was used to be filtered via a syringe filter having pore size of 0.45 μ m, in order to remove excessive catalyst in the sample. This sampling process continued up to 180 minutes.

2.4.1. Optimization Studies

Experiments were performed by changing the parameters like solution pH, pollutant concentration and catalyst dose to select the best dose and catalyst for photocatalytic degradation. All photocatalytic experiments were performed in duplicates.

2.4.2. Catalytic dose Experiments

Experiments were performed by using five different doses of catalysts ranging from 0.25 to 1.5 g/L (i.e., 0.25, 0.5, 0.75, 0.1, and 1.5 g/L) in order to check the optimum dose by keeping other settings same like experimental time duration, initial pH, light source and MO concentration as 50 mgL⁻¹.

2.4.3. Point of Zero Charge

Point of zero charge of a catalyst is the point where its surface is electrically neutral or has zero charge. The surface of catalyst is positively and negatively charged below and above that specific point. To find the pHPZC of catalysts, the salt addition method was chosen, where 0.1M KCl solution was used as solvent. About 20 mL of 0.1M KCl was added in five borosilicate glass beakers and catalyst dose of 2 g/L was added in each beaker after adjusting the pH at 3, 5, 7, 9 and 11 using 0.5 M HCl and 0.5 M NaOH while the suspensions were left for 24 h at room conditions. At 24th h the pH of suspensions was

measured and graphs of obtained values plotted against initial pH values of KCl solution, provided the pH_{PZC} value for the catalyst (Hanif et al., 2022).

2.4.4. pH of Solution Experiment

The pH of solution is an important factor to test the catalytic activity. After the selection of most active catalyst at its optimum dose (1g/L for ternary composite), pH experiments were carried out to check the impact of solution pH, maintained at 3, 5, 7, 9 and 11 respectively. During the experiments, reaction time, methyl orange concentration and catalyst dose were kept constant, while 0.5M HCl and 0.5M NaOH were used to sustain pH.

2.4.5. Concentration of Solution Experiment

The concentration of the solution is critical in determining a composite's photocatalytic degradation capacity. Following the determination of the optimal pH of 5, as well as the specific fraction of the ternary composite exhibiting the highest activity among various fractions, and a catalyst dose of 1g/L, the next phase of the experimentation involved investigating the influence of solution concentration on the degradation of the pollutant (methyl orange). This was accomplished by using methyl orange concentrations of 25mg/L, 50mg/L, 75mg/L, and 100mg/L. The delicate relationship between solution concentration and photocatalytic performance was comprehensively studied through this systematic investigation, providing vital insights into the composite's potential for percentage degradation of pollutant.

2.4.6. Characterizations

In order to analyse the crystal structure and its purity, a non-destructive technique X-ray diffraction was employed (XRD, Bruker AXS- D8, Germany) using Cu-K α ($\lambda = 1.5406$ nm) as source of radiation and secondary monochromator in the range 2θ from 10 to 80°. During analysis, the crystalline material, grounded in powder is kept in the path of X-ray radiation where it diffracts through the crystal planes and detector while the radiation and detector rotate through an angle range. To test the chemical or elemental composition of materials EDAX were performed using Omicron system (Al K α 1486.7 eV X-ray source operated at 15 KeV). Surface morphology and physical characteristics of as prepared nano-

catalysts was obtained by using Scanning Electron Microscope (SEM) (Hitachi S 4800) at an operating voltage of 25 KeV. SEM. Transmission Electron Microscopy (TEM) were implemented on a JEOL (JEM-2100) electron microscope operating at the voltage of 20 kV.

3. RESULTS AND DISCUSSION

3.1. Characterization Results of Nanocatalysts

3.1.1. X-ray Diffraction

To analyze structural phase and crystallinity of particles the X-ray Diffraction of prepared powder was performed. XRD patterns of BiVO₄, HMT, g-C₃N₄, and 15% (BiVO₄/HMT@g-C₃N₄) are given in **Figure 3.1**. X-ray diffraction spectra of pure BiVO₄ materials showed the same as diffraction peaks pattern of Joint Committee on Powder Diffraction Standards (JCPDS#75-1866) that is ascribed to monoclinic scheelite structure of BiVO₄. The (110), (011), (121), (040), (200), (002), (051), (240), (200), (042), (202), (161), (321), (123) was obtained to the corresponding angles 18.90°, 19.04°, 29.27°, 32.76°, 36.73°, 37.20°, 42.78°, 44.75°, 48.95°, 49.14°, 53.43°, 56.60°, 62.67°, and 63.87° respectively. The intense peaks appeared at $2\theta = 19.04^\circ$ and 29.27° indexed to hkl values of (011) and (121) respectively (Shafiq et al., ., 2022). The XRD pattern of hydrogen peroxide modified Titanium oxide (HMT) shows pattern of anatase, and rutile correspond to the patterns in JCPDS#88-1175(anatse) and JCPDS#84-1268(rutile) respectively. The rutile phase shows peaks at 27.4°, 36.0°, 41.2°, 44.0°, and 56.6° that correspond to the (110), (101), (111), (210), and (220) planes of both samples respectively. The antase phase contain peaks at 25.2°, 37.7°, 48.0°, 53.8°, 55.0°, and 62.6° that correspond to the (101), (004), (200), (105), (211), and (204) planes of both samples respectively (Han et al., 2018; Rashid et al., 2022). Two distinct diffraction peaks in XRD pattern of g-C₃N₄. The graphitic planes in g-C₃N₄ are constructed from tri-s-triazine building units. The peak pattern indexed to JCPDS#87-1526 which is for hexagonal phase of g-C₃N₄. The characteristic diffractions at 13.1° and 27.5° indexed to (100) and (002) peaks, which are originated due to interlayer stacking aromatic segments of bare g-C₃N₄ (Zhu et al., 2014). The distinct diffraction peaks observed in 15% ternary composite pattern attributed to the crystalline phases in composite. The broadening of some peaks may suggest the presence of smaller nanoscale domains and absence of some major peak shifts in the composite suggests that the synthesis process maintains the integrity of the individual constituents while forming ternary composite. Graphitic carbon nitride (g-C₃N₄) is base material in 15%

ternary composite, so it has distinct diffraction peak in the pattern. The presence of well-defined peaks suggests that BiVO_4 @HMT particles are deposited on $\text{g-C}_3\text{N}_4$. Therefore, the XRD results confirm the successful preparation of BiVO_4 @HMT/ $\text{g-C}_3\text{N}_4$ ternary composite.

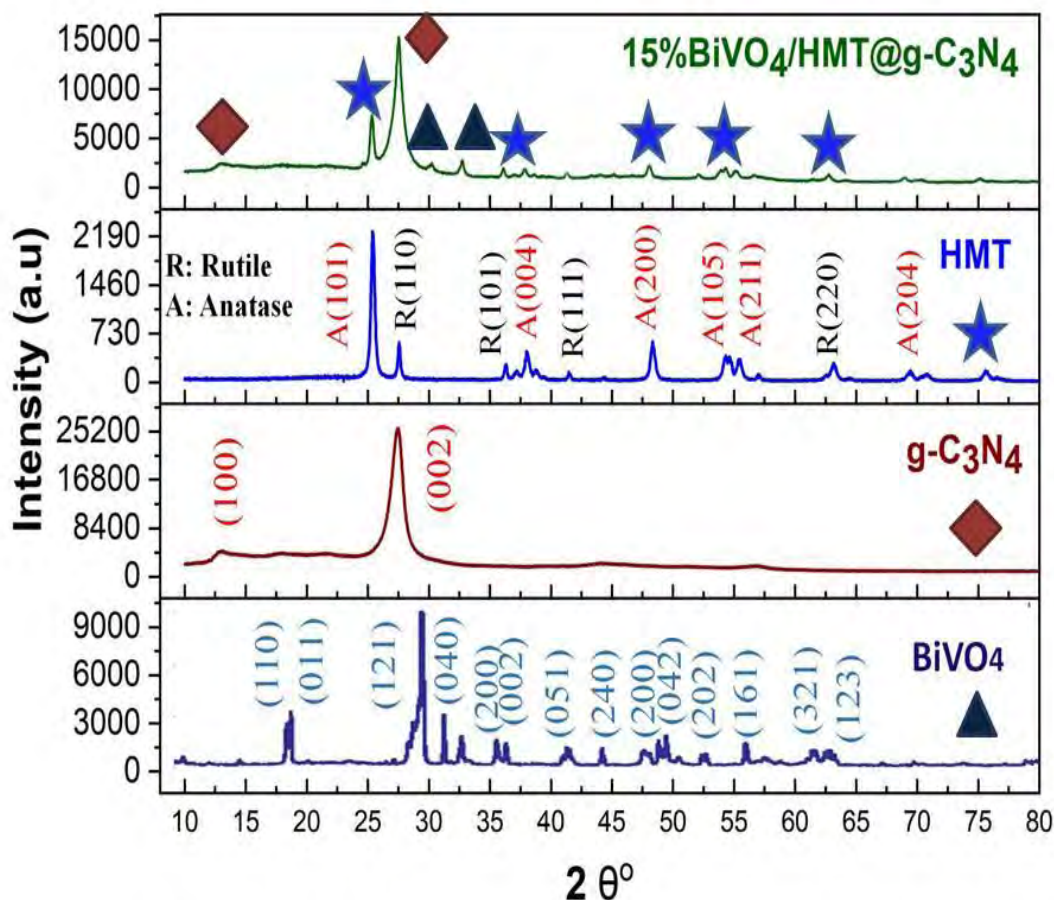


Figure 3.1: XRD patterns of BiVO_4 , $\text{g-C}_3\text{N}_4$, HMT, and 15% (BiVO_4 @HMT/ $\text{g-C}_3\text{N}_4$).

3.1.2. Morphological Assessment of Nano-catalyst

3.1.2.1. Scanning Electron Microscopy

The morphological details and the uniform size distribution of synthesized nano materials were observed through scanning electron microscope images as shown in **Figure 3.2**. The **Figure 3.2(a)** shows agglomerated spindles like shapes of BiVO_4 material. The calcining temperature has great influence on structure of BiVO_4 and agglomeration of particles increase with increase in temperature. Furthermore, it is reported that size of particles 0.3-

0.5 μm , 0.5-0.7 μm and 0.7-1.0 μm for temperature 400 $^{\circ}\text{C}$, 500 $^{\circ}\text{C}$, and 600 $^{\circ}\text{C}$, respectively (Pookmanee et al.,2013). **Figure 3.2(b)** shows SEM image of typical multilayer stacking structure of g-C₃N₄ powder, confirming graphitic nature of carbon nitride. Additionally, it is reported that calcination of melamine at 400 $^{\circ}\text{C}$ to 500 $^{\circ}\text{C}$ results typical slaked layered structure and slate like morphology is observed in diameters of approximately 50-200 nm (Chang et al.,2013; Ma et al.,2016; Yang et al.,2017). **Figure 3.2(c)** shows morphology of hydrogen peroxide modified titania. Images show that the particles are nearly homogenous in size and shape, with dimensions in the nanometer range. These particles continue to be arranged in a coherent pattern. However, it is difficult to distinguish the individual forms of the particles, because of the imaging instruments' resolution limitations and the potential of particles clustering during the preparation process (Rashid et al., 2022). **Figure 3.2(d)** The SEM image illustrates agglomeration phenomenon of BiVO₄@HMT particles and reveals distribution of particles of binary composite (BiVO₄@HMT) on surface of lamellar structure of g-C₃N₄ sheets. The morphology of SEM images of pure BiVO₄, HMT, g-C₃N₄, and ternary composite (BiVO₄@HMT/ g-C₃N₄), confirming the synthesis of nano materials and deposition of (BiVO₄@HMT) on g-C₃N₄.

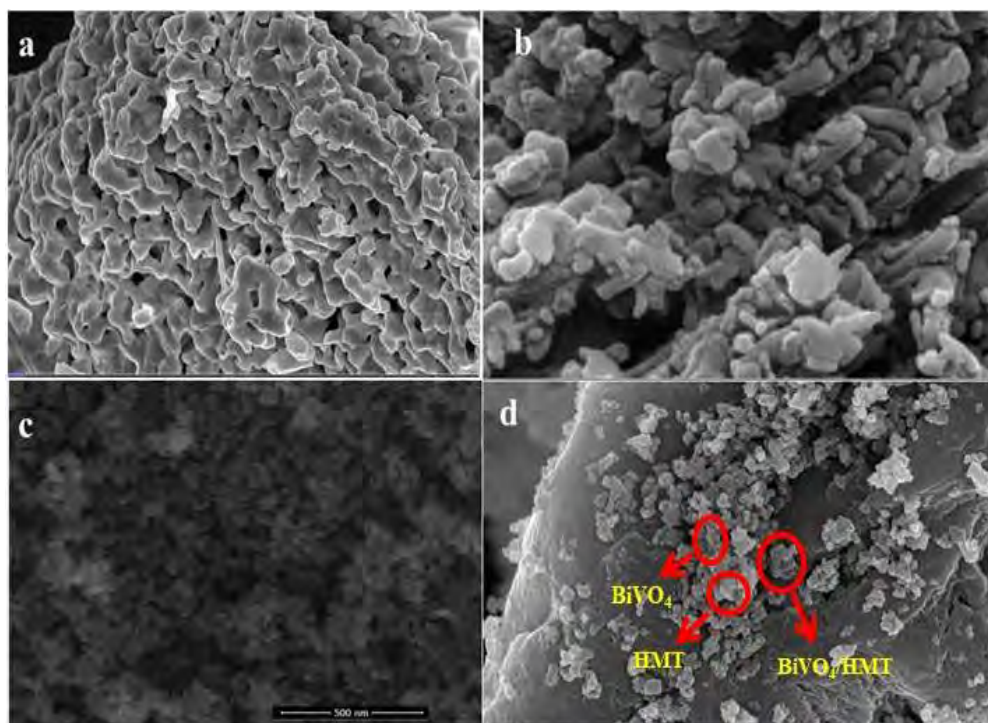


Figure 3.2: (a) SEM image of BiVO_4 , (b) SEM image of gC_3N_4 , (c) SEM image of HMT, (d) SEM image of 15% ($\text{BiVO}_4@$ HMT/ gC_3N_4) ternary composite.

3.1.2.2. Transmission Electron Microscopy

To further unveil microstructure of ternary composite, TEM investigation was performed. In **Figure 3.3** the TEM image shows good assembly of BiVO_4 nano particles and HMT crystals on surface of $\text{g-C}_3\text{N}_4$ sheets. Crystals of $\text{g-C}_3\text{N}_4$ and HMT are prominent, less than diameter of 100 nm. Image shows sharp rectangular crystals of HMT and round particles of BiVO_4 on wide sheets of $\text{g-C}_3\text{N}_4$. Dark areas are due to denser deposition of ($\text{BiVO}_4@$ HMT) particles on $\text{g-C}_3\text{N}_4$.

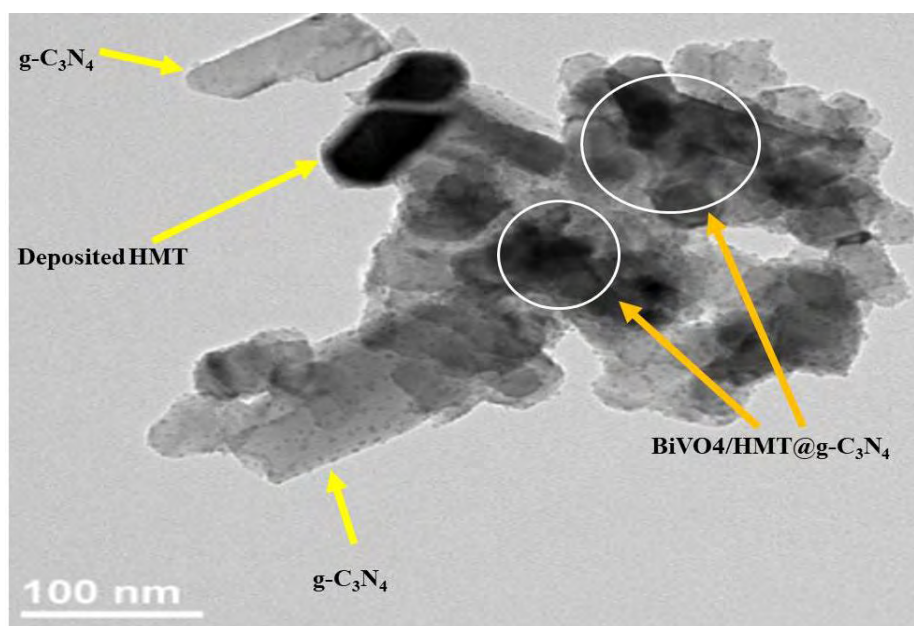


Figure 3.3: TEM image of Ternary Composite ($\text{BiVO}_4@$ HMT/ $\text{g-C}_3\text{N}_4$).

3.1.3. Elemental Composition Analysis

The chemical composition and purity of as prepared nano composite were analyzed through energy dispersive X-ray spectroscopy (**Figure 3.4**). The EDS confirms the presence of Bi, V, O, Ti, C, and N in the ternary composite. It confirms the formation of ternary composite without impurities. The elements of Bi, V, and O were showing energy levels of $K\alpha = 2.42, 4.95,$ and 0.52 keV, respectively (Longchin et al., 2016) and peaks around 1keV and around 5keV can be attributed to Ti (Rashid et al., 2022).

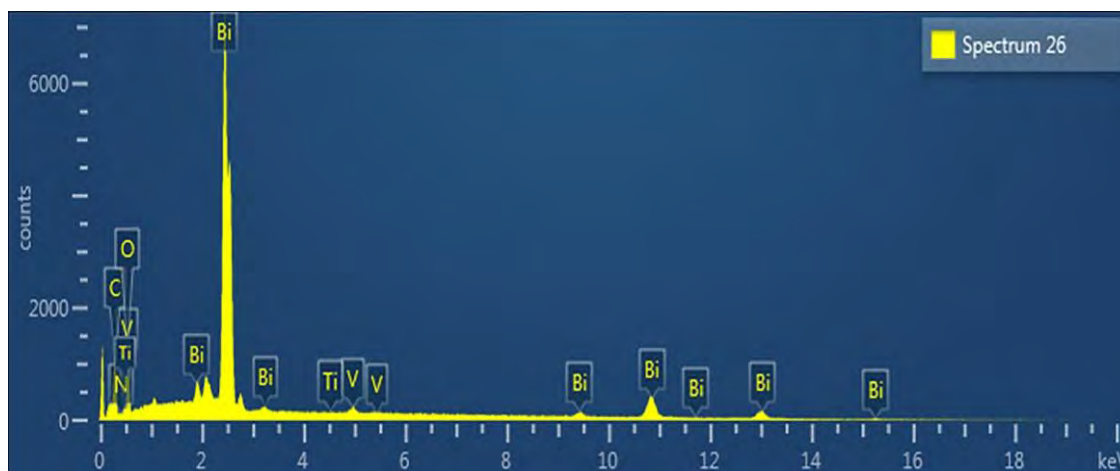


Figure 3.4: EDS spectrum of 15% ternary composite ($\text{BiVO}_4\text{@HMT/g-C}_3\text{N}_4$).

3.1.4. Optical Properties and Band Gap Analysis

The light absorption and band gap energy of BiVO_4 , HMT, $\text{g-C}_3\text{N}_4$, and 15% ($\text{BiVO}_4\text{@HMT/g-C}_3\text{N}_4$) ternary composite observed by UV-vis absorbance spectroscopy measurement. **Figure 3.6(a)** shows absorption spectra of BiVO_4 , $\text{g-C}_3\text{N}_4$, and 15% ($\text{BiVO}_4\text{@HMT/g-C}_3\text{N}_4$). It is seen that absorption edge of BiVO_4 is at ~ 650 nm, and that of $\text{g-C}_3\text{N}_4$ is at ~ 490 nm. The adsorption edge of HMT is reported at ~ 400 nm (Rashid et al., 2022). All synthesized material absorbance located in visible region. The visible-light absorbance ability obtained through Tauc's relationship which shows that 15% ternary composite has better light harvesting efficiency than pure $\text{g-C}_3\text{N}_4$, which is beneficial to the enhancement of photocatalytic performance. **Figure 3.6(b)**. The Tauc plots of BiVO_4 , $\text{g-C}_3\text{N}_4$, and 15% ($\text{BiVO}_4\text{@HMT/g-C}_3\text{N}_4$) calculated from $(\alpha h\nu)^{1/2}$ versus $h\nu$ to determine their band gap E_g (Norouzzadeh et al., 2020). As shown 15% ternary composite had smaller band gap as compared to pure $\text{g-C}_3\text{N}_4$. The decrease in band gap can be explained as formation of heterojunction between the three components that can be activated by visible light irradiation.

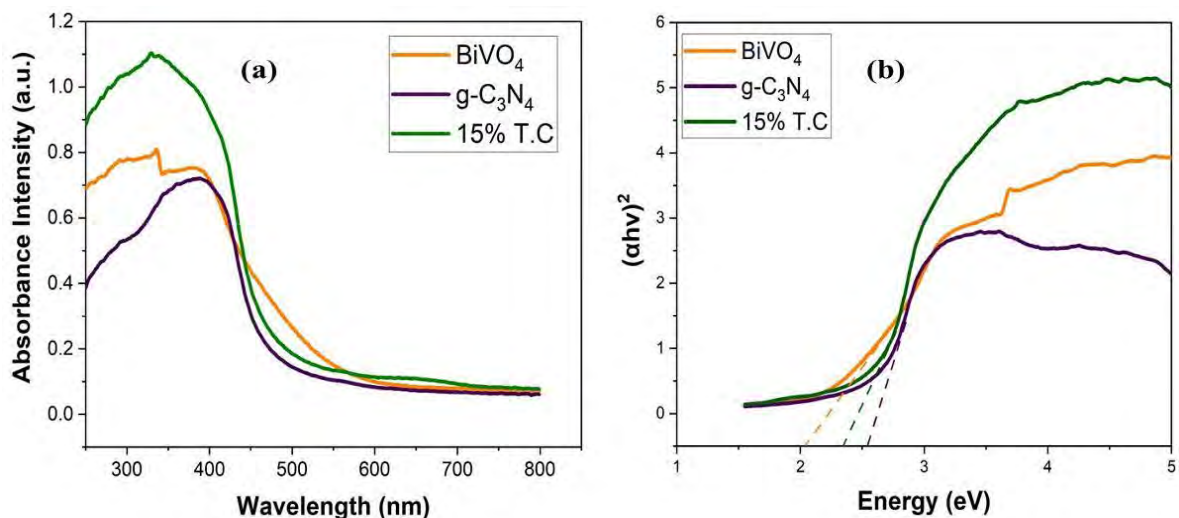


Figure 3.5: (a) UV-visible absorbance spectra of pure BiVO₄, g-C₃N₄, and 15% BiVO₄@HMT/g-C₃N₄; (b) Tauc plot of BiVO₄, g-C₃N₄, and 15% BiVO₄@HMT/g-C₃N₄.

3.2. Calibration Curve of Methyl Orange

Straight line equation for methyl orange calibration curve by UV-visible spectrophotometer $y = 0.0393x - 0.0521$ (**Figure 3.6**). The value of $m = 0.0393$ and value of $c = -0.0521$. R^2 value was calculated to be 0.9965. UV-visible spectrophotometer was used for spectral scanning of samples from 200 to 800 nm wavelength range. 25 mg/L methyl orange was the highest methyl orange concentration detectable by UV-visible spectrophotometer.

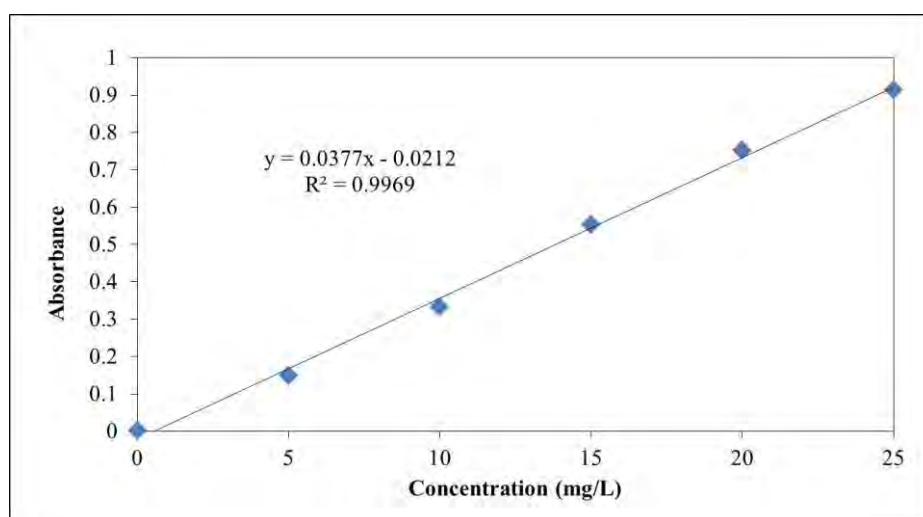


Figure 3.6: Calibration Curve of Methyl Orange Dye standards

3.3. Preliminary Studies

To investigate degradation potential of pure BiVO_4 , HMT, $\text{g-C}_3\text{N}_4$, and different percentage of binary and ternary composite photocatalyst, a solution containing 25 mg/L concentration of methyl orange dye was used. The working solution was 100 mL from stock solution, pH of solution was 6.58 and dose of catalyst was 1 g/L. As shown in **Figure 3.7** pure BiVO_4 had highest potential of degrading pollutant up to 51%, followed by HMT which degraded up to 44.56% during duration of 180 min and $\text{g-C}_3\text{N}_4$ has minimum degradation potential (36.56%) of methyl orange. However, the study conducted in the absence of the catalyst showed negligible degradation of methyl orange dye even after 180 min of irradiation. The superior degradation rate of MO by BiVO_4 is due to its lower band gap, small particle size, and high oxygen vacancy density according to reported literature (Liu et al., 2017; Ying et al., 2015).

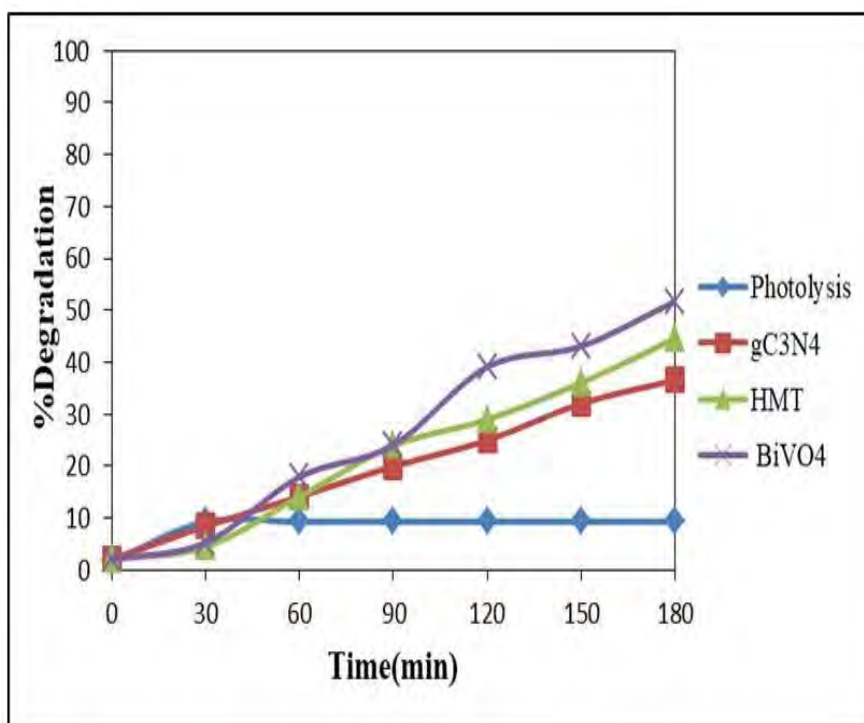


Figure 3.7: Degradation of MO using pure BiVO_4 , HMT, $\text{g-C}_3\text{N}_4$, and photolysis

Figure 3.8 depicts results of experiment for percentage degradation of MO using different fractions (5%, 10%, 15%, 20%, and 25%) of binary composite (BiVO_4/HMT). It is evident that 25% BC exhibits highest photocatalytic degradation efficiency after visible light

irradiation for 180 min. While 5% BC had the lowest efficiency of photocatalytic degradation as compared to other fractions of binary composites. A blank experiment in absence of binary composite demonstrates that no obvious change in concentration of methyl orange was found. In our results, the photocatalytic activity of the binary composite ($\text{BiVO}_4\text{@HMT}$) increased with increase in BiVO_4 fraction from 5 to 25%. The 25% BC might favored electron-hole pair migration that lead to high photocatalytic activity as reported in a study where BiVO_4 increased photocatalytic activity in binary composite (Zhao et al., 2016). In another study reported by Mane and colleagues (Mane et al., 2022) photocatalytic activity of the binary composite increased with raised doped fraction of BiVO_4 thus leading to enhanced MO degradation, attributed to the increase in number of active sites of binary composite.

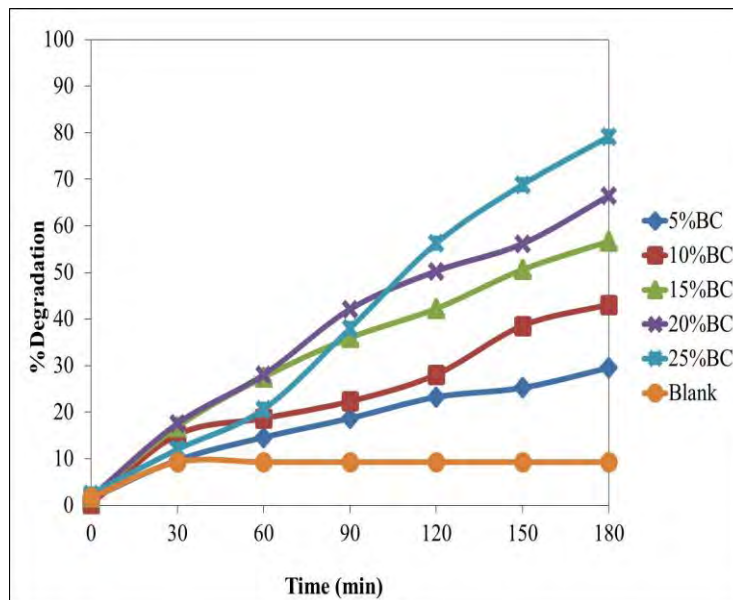


Figure 3.8: Percentage degradation of MO by binary composite ($\text{BiVO}_4\text{@HMT}$) fractions.

Figure 3.9 shows experimental results for degradation of pollutant by ternary composites with fractions of the 25% binary composite (5%, 10%, 15%, 20%, and 25%). The blank experiment results in **Figure 3.9** spectacles that MO is hardly degraded under visible light irradiation without photocatalyst. In the presence of 5% ternary composite ($\text{BiVO}_4\text{@HMT/g-C}_3\text{N}_4$) nanoparticles, about 37% of pollutant was degraded after 180 min of exposure, indicating weak photocatalytic activity. While 15% binary composite fraction in the ternary composite showed highest photocatalytic activity among all composites. In

these composites, the photocatalytic activity gradually increases with increasing ($\text{BiVO}_4@\text{HMT}$) fraction and highest value of degradation achieved with 15% $\text{BiVO}_4@\text{HMT}/\text{g-C}_3\text{N}_4$, which is about 80% degradation percentage of methyl orange after irradiation for 180 min. Further increase in fraction of $\text{BiVO}_4@\text{HMT}$ showed decrease in degradation potential that is maybe due to agglomeration of particles over gC_3N_4 . The results of this study are in good coherence with reported literature as its reported that $\text{g-C}_3\text{N}_4$ based ternary composites can significantly modify physiochemical and photocatalytic properties toward MO dye degradation (Aljuaid et al., 2023; Kamble et al., 2023).

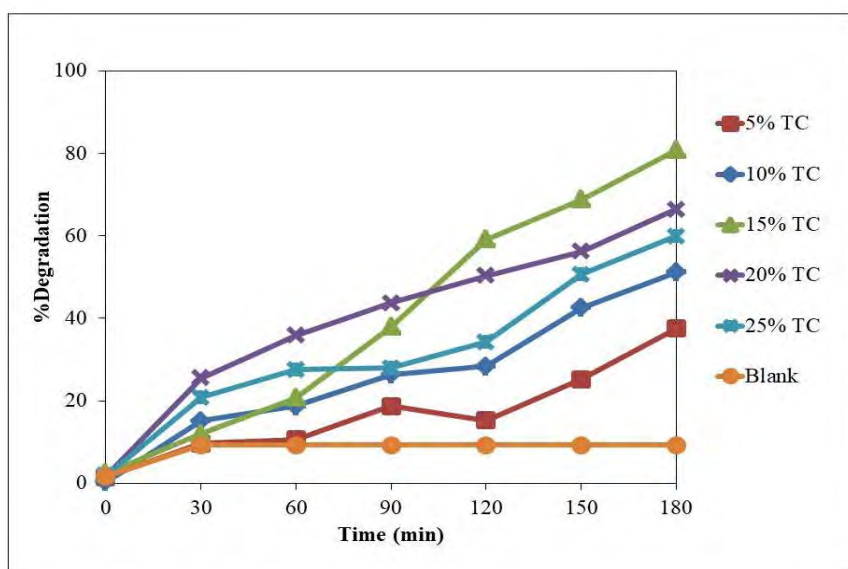


Figure 3.9: Degradation of MO over ternary composite ($\text{BiVO}_4@\text{HMT}/\text{g-C}_3\text{N}_4$)

3.4. Optimization Studies

3.4.1. Point of Zero Charge

The pH, at which net charge on catalyst surface is zero or surface is electrically neutral, is called pH_{PZC} . While the surface of catalyst is in positive or negative charge below or above pH_{PZC} value, respectively (Hanif et al., 2022). In this study to estimate pH_{PZC} of the prepared 15% ternary composite, the pH drift technique was used. The initial pH (pH_i) of the solution was adjusted by adding either 0.5 M HNO_3 or NaOH . Followed by addition of 15% ternary composite and after 24 hours final pH (pH_f) was then measured. The pH_{PZC} was found by plotting pH_i vs ΔpH ($\text{pH}_f - \text{pH}_i$) and pH_{PZC} is a point at which total number

of negative and positive charges are equal. The pH_{PZC} value of 15% ternary composite was 6.83 (Figure 3.10). The results show that the catalyst's surface has negative charge at higher pH than value of pH_{PZC} and positive charge at lower pH values than pH_{PZC} .

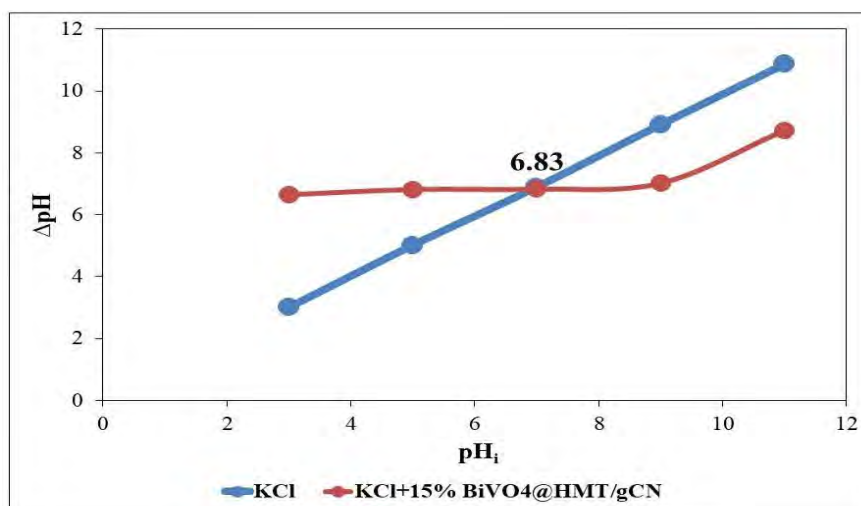


Figure 3.10: Point of zero charge of 15% ternary composite.

3.4.2. Effect of Solution pH

The pH of solution is one of most important parameters for controlling photo-catalytic degradation of methyl orange. The pH effect of the as prepared 15% ternary composite for photocatalytic degradation of methyl orange was investigated at five different pH values (3, 5, 7, 9, and 11). Additionally, the catalyst dose (1 g/L) and solution concentration 50 mg/L in each experimental were same. (Figure 3.11) shows the result influence of initial pH solution on the methyl orange degradation by 15% ternary composite. The highest percentage degradation of methyl orange (84.30%) was found to be at pH 3. The photocatalytic degradation percentage decreased to 79.52%, 59.78%, 41.78%, and 30.74% with increase in the solution pH value to pH 5, pH 7, pH 9, and pH 11, respectively. The catalyst's surface is positively charged below pH_{PZC} and methyl orange is an anionic dye. Methyl orange degradation is favored in acidic medium due to presence of N-H group that easily interacts and create strong electrostatic attraction with positively charged catalyst surfaces (Hanif et al., 2022). Additionally, during photoreactions, presence of hydroxyl radicals demolishes methyl orange molecules as there is no deposition of methyl orange molecules on catalyst surfaces (Hanafi et al., 2020).

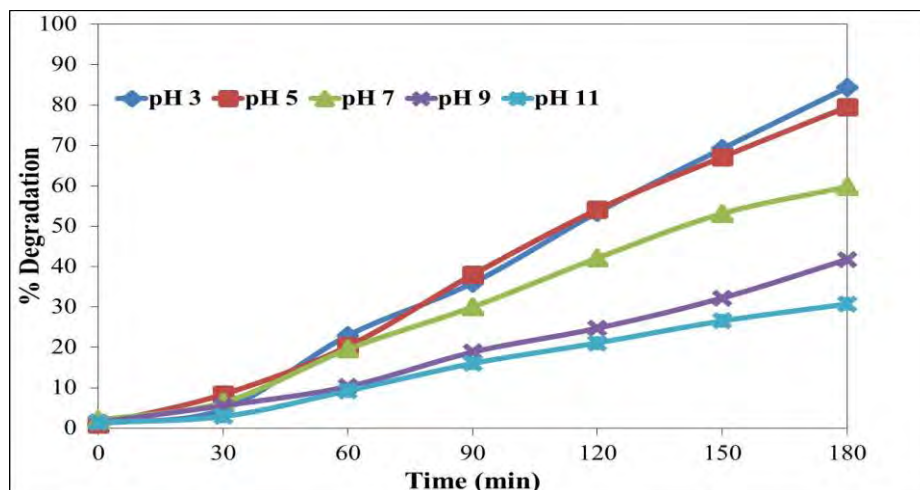


Figure 3.11: Effect of pH on degradation of methyl orange under visible light

3.4.3. Effect of pollutant concentration

The concentration of pollutant is an important factor that influences photocatalytic degradation of methyl orange. Four different concentrations (25, 50, 75, and 100 mg/L) of MO were used and 1 g/L of the ternary photocatalyst dose was used at pH5 for all experiments. As shown in **Figure 3.12**, as we increase concentration of pollutant, decrease in percentage degradation can be observed. The highest photocatalytic degradation of methyl orange at given conditions observed for 25 mg/L solution concentration. The decrease in efficiency of nanocomposite with increase in MO concentration is generally ascribed to the decreased active sites as well as light screening effect owing to higher dye concentration. Some literature also report it with fact of adsorption of reactants on the catalyst surface. These observations are in good agreement to already reported photocatalytic degradation of MO (Naikwade et al., 2020; Sajid et al., 2021).

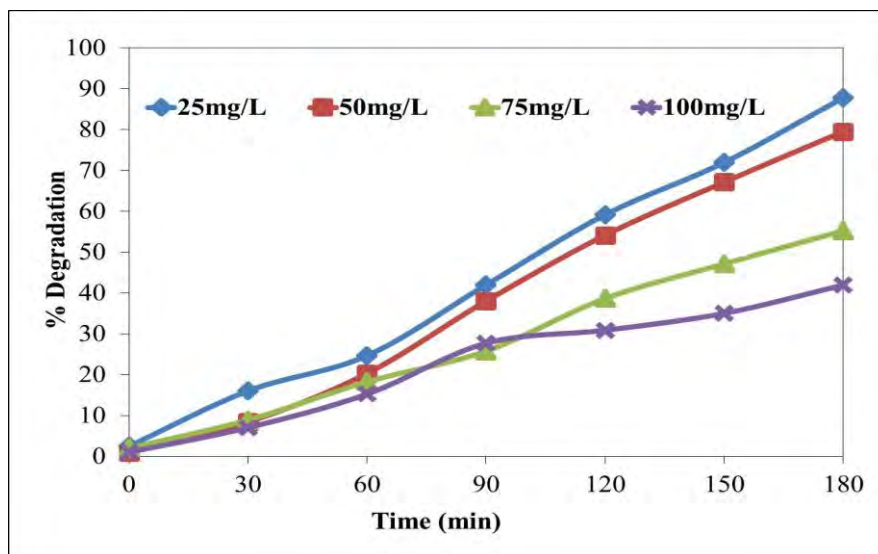


Figure 3.12: Effect of pollutant concentration on degradation of MO under visible light using 15% $\text{BiVO}_4@\text{HMT}/\text{g-C}_3\text{N}_4$ at pH 5.

3.4.4. Effect of Photo-Catalyst Dose

To figure out photocatalytic degradation efficiency of photocatalyst, dose of photocatalyst is important, which gives idea about the maximum degradation of pollutant using minimum amount of catalyst dose. Experiments were carried out by varying photocatalyst dose 0.25, 0.5, 0.75, 1.0, and 1.5 g/L for pollutant concentration 50 mg/L at pH 5. As shown in **Figure 3.13** a steep increase in percentage degradation of MO until catalyst dose reached up to 1 g/L and further increase in dosage of catalyst resulted in decrease of photocatalytic degradation efficiency after 180 min of irradiation time. The decrease in photocatalytic activity might be endorsed to light screening effect, hidden active sites due to catalytic agglomeration and sedimentation of the nanoparticles due to higher loading, respectively (Liu & Perng, 2020; Phadi et al., 2021).

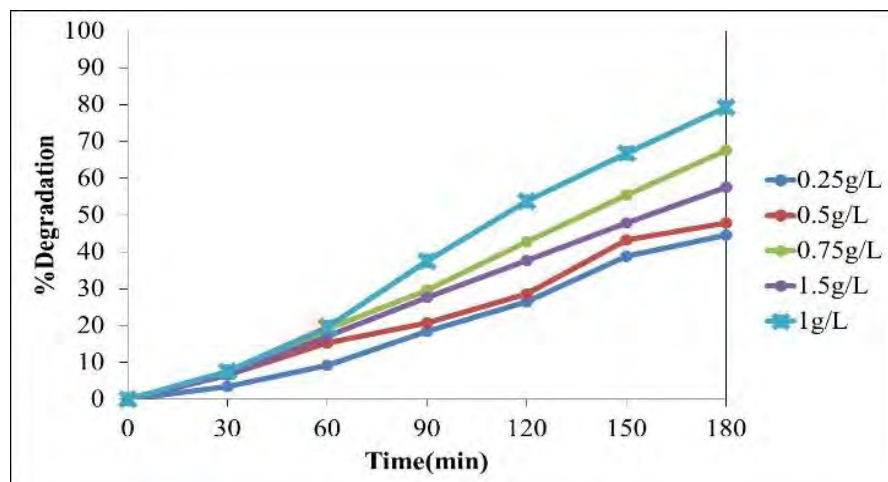


Figure 3.13: Effect of dose of photo-catalyst on photo degradation of MO dye.

3.4.5. Reusability

In this work, the catalyst was used 3 times with three times recycling; the respective efficiency of which was found to be 79.32%, 78.1% and 70.98%. The decrease of percentage degradation after second time use may be due to the loss of some quantity of catalyst during filtration. Agglomeration and sedimentation of the dye around ternary composite's particles after each cycle of photocatalytic degradation is another possible cause of the observed decrease in the degradation rate because each time the photo-catalyst is reused the new parts of the catalyst surface become unavailable for dye adsorption and thus photon absorption, reducing the efficiency of the catalytic reaction (Tadesse et al., 2021).

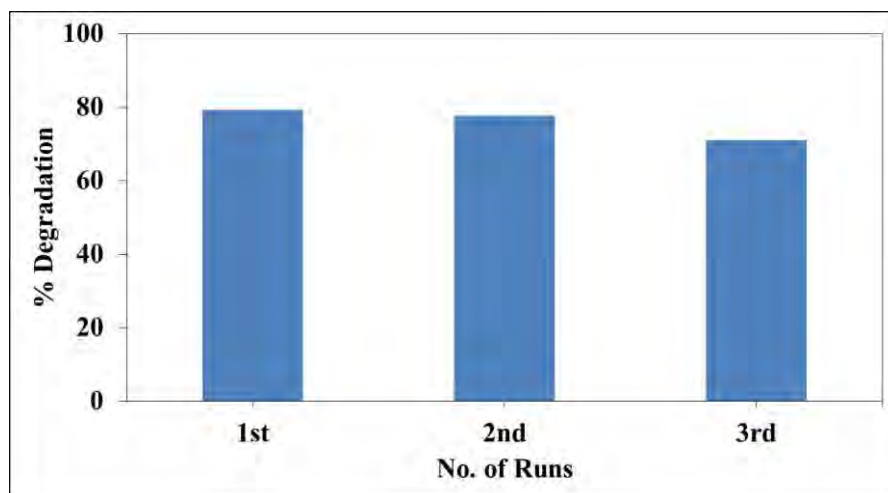


Figure 3.14: Reusability of 15% TC for photo degradation of MO

This study investigated the degradation of methyl orange utilizing different photocatalysts, including BiVO₄, HMT, and g-C₃N₄. Through a systematic approach, binary composites of BiVO₄ and HMT, as well as a ternary composite comprising BiVO₄, HMT, and g-C₃N₄, were prepared. Experiments were carried out to optimize key parameters such as fraction, pH, dose, and concentration. Notably, the degradation of methyl orange was effectively achieved under visible light irradiation. Remarkably, the highest degradation rate of 79.32% was achieved at a pH of 5, a composite dose of 1g/L, and a dye concentration of 50 mg/L, while pristine g-C₃N₄, HMT, and BiVO₄ achieved degradation rate upto 38.26%, 40.74%, and 51.68% respectively. Comparisons between the ternary composite and bare g-C₃N₄, HMT, and BiVO₄ revealed the former's superior performance. Impressively, the ternary composite exhibited reusability for up to three cycles, with the final run achieving a degradation rate of 70.98%. This study's findings underscore the efficacy and potential of the novel ternary composite as a promising solution for the degradation of methyl orange and highlight its potential for sustainable wastewater treatment.

3.4.6. Reaction Kinetics Studies

The determination of the kinetics and the influence of physiochemical parameters are important to determine degradation rate. In this context, different studies using pristines, ternary composite, pH, Dose, and pollutant concentration with various conditions were carried out. The photocatalytic degradation rate of MO dye follows the pseudo-first-order kinetics model as quantified by using the following relation:

$$\ln \left(\frac{C_t}{C_o} \right) = -kt$$

Here, $-k$ is rate constant, $-C_o$ is initial concentration of MO dye and $-C_t$ is concentration of MO dye at time $-t$. Moreover, comparison between pseudo first order and second order kinetics model is illustrated in **Table 3.1**. The apparent rate constant (K_{app}) values that has been derived from the slope of their regression plots and regression coefficient (R^2) revealed that photocatalytic degradation of ibuprofen perfectly follows the pseudo first-order kinetics.

Reaction kinetics for operational parameters like effect of BiVO₄@HMT (binary composite) loading on g-CN, effect of solution pH, effect of pollutant concentration and effect of catalyst dose were studied. Results revealed that 15% loading of binary composite on g-CN gave the highest rate constant value (0.009 min⁻¹) (**Figure 3.15**) having R² = 0.98. Moreover, it was also observed that an increase in solution pH lead to decrease in reaction rate constant from 0.009 min⁻¹ to 0.002 min⁻¹ for pH 5 to pH 11 (**Figure 3.16**), respectively. Highest reaction rate observed at pH 5 proved that acidic condition favors the degradation of MO dye because at lower pH value, surface of catalyst is probably positively charged while the pollutant's anionic nature has already been discussed in section 3.4.2. Impact of increased pollutant concentration was also assessed and rate constant values are given in **Table 3.1**, where the K (min⁻¹) value for 50ppm was calculated to be 0.004 min⁻¹ with highest R² value of 0.98 (**Figure 3.17**) while for the higher concentrations like 75ppm and 100ppm, its value got decreased till 0.97 and 0.95, accordingly. It can be attributed to decrease in photocatalytic efficiency and higher selectivity of catalyst for intermediates as compared to parent compound, while in literature several studies have suggested that photocatalytic degradation rate of organic pollutants is linearly dependent on initial substrate concentration (Yang et al., 2016). Catalyst's dose studies (**Figure 3.18**) exhibited that reaction rate constant values increased from 0.003 min⁻¹ to 0.008 min⁻¹ with the increase in catalyst dose which proved that increase in catalyst dose increases the number of available active sites on catalyst's surface which enhances the formation of radical species that promote the photodegradation (Behzadifard et al., 2018).

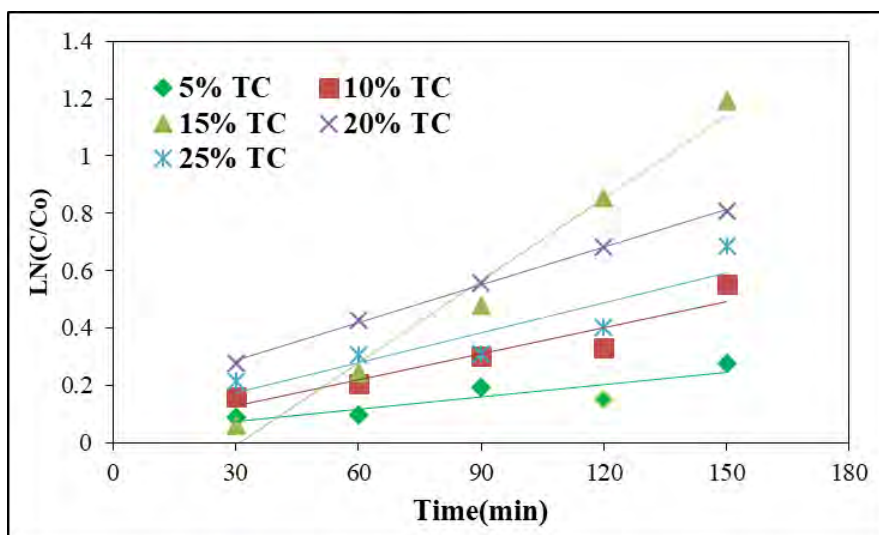


Figure 3.15: Photodegradation kinetic plot showing the effect of binary composite loading (catalyst dose = 1g/L, MO concentration = 25mg/L)

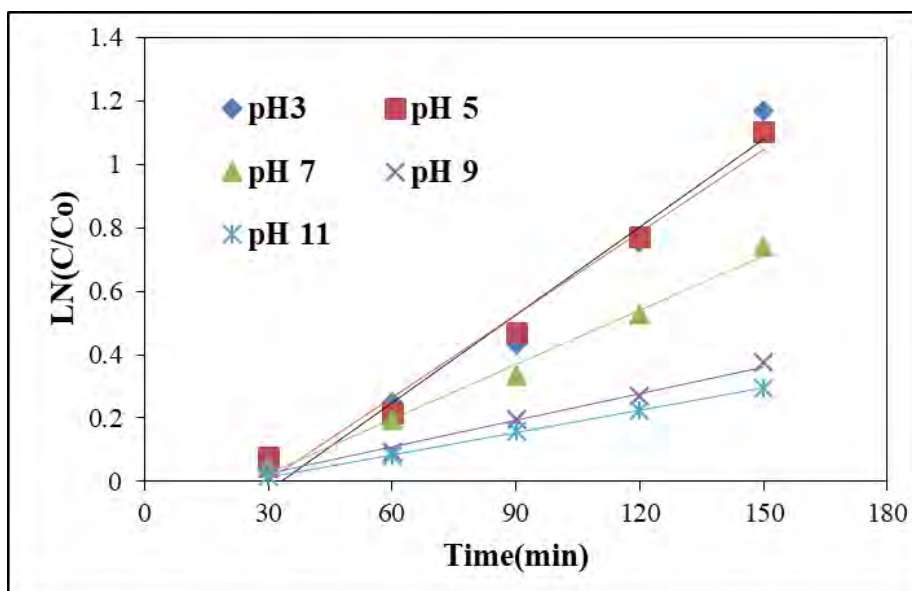


Figure 3.16: Photodegradation kinetic plot at different pH values (catalyst = 15% T.C, Dose = 1g/L, MO concentration = 50 mg/L)

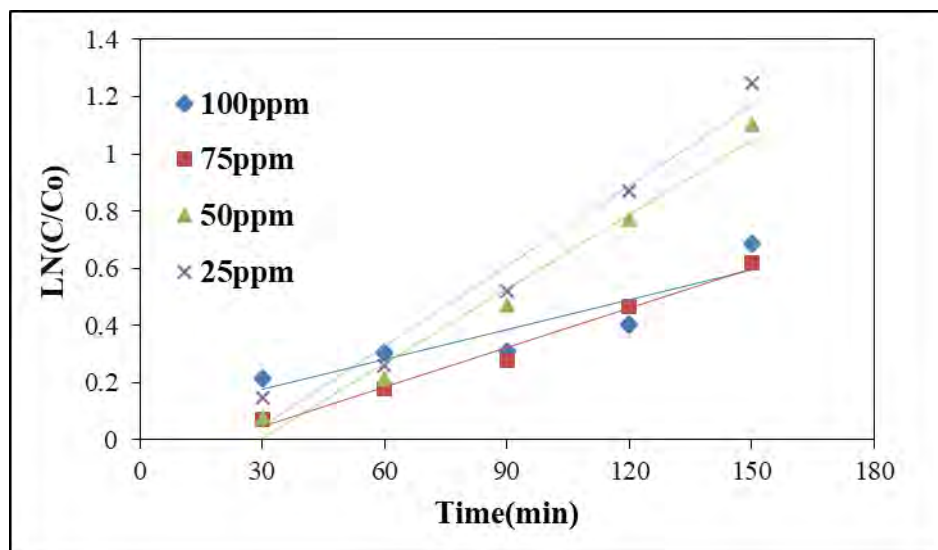


Figure 3.17: Photodegradation kinetics plot at different pollutant concentrations (catalyst = 15% T.C, Dose = 1g/L, pH = 5)

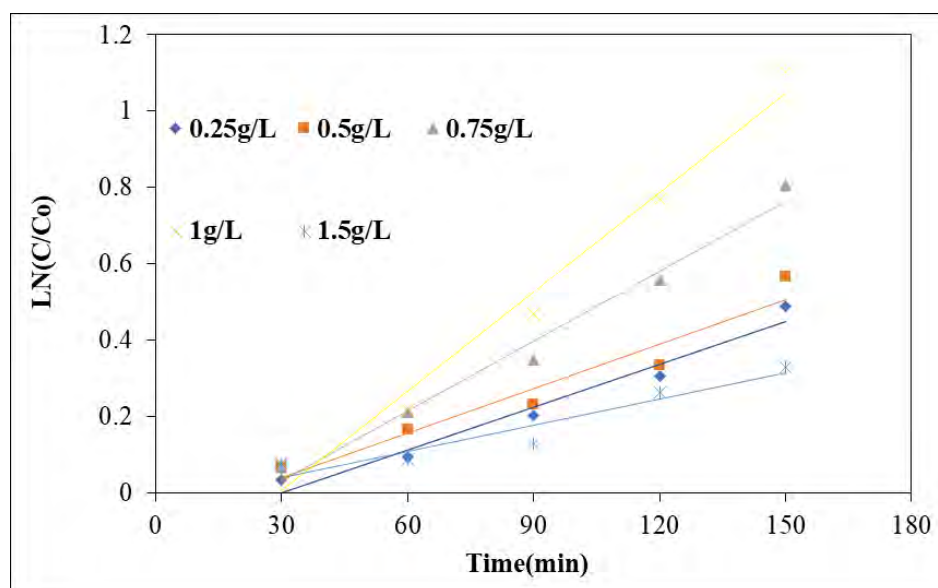


Figure 3.18: Photodegradation kinetics plot at different doses (catalyst = 15% T.C, MO concentration = 50 mg/L, pH = 5)

Table 3.1. Comparison between pseudo first order, second order and Pseudo First kinetics applied on different operational parameters.

Sr. No	Studies	Conditions	First Order Kinetics		Second Order Kinetics		Pseudo First Order Kinetics		
			K (min ⁻¹)	R ²	K (min ⁻¹)	R ²	K (min ⁻¹)	R ²	
1	Pristines	1g/L Dose							
			BiVO₄	0.004	0.976	0.0002	0.954	0.004	0.976
	HMT	1g/L Dose	0.004	0.978	0.0002	0.952	0.004	0.976	
		1g/L Dose							
			g-C₃N₄	0.003	0.976	0.0001	0.9631	0.003	0.9776
2	Ternary	5%	0.002	0.8612	0.0001	0.824	0.002	0.8702	
		10%	0.004	0.9437	0.0002	0.9086	0.004	0.9481	
	Composites	15%	0.009	0.9437	0.0009	0.8256	0.009	0.98	
		20%	0.005	0.9266	0.0004	0.9532	0.005	0.9531	
		25%	0.004	0.9199	0.0003	0.8667	0.004	0.9199	
		3	0.01	0.9207	0.0005	0.7627	0.01	0.9207	
	3	pH	5	0.009	0.9451	0.0004	0.8205	0.009	0.9451
			7	0.005	0.98	0.0002	0.944	0.005	0.98
9			0.003	0.9654	0.00008	0.9338	0.003	0.9654	
11			0.003	0.9654	0.00005	0.9811	0.002	0.9868	
100ppm			0.003	0.9431	0.0002	0.954	0.004	0.9599	
4	Pollutant Concentration	75ppm	0.004	0.97	0.00009	0.9447	0.009	0.9751	
		50ppm	0.009	0.9451	0.0004	0.8205	0.004	0.98	
		25ppm	0.01	0.9003	0.001	0.6886	0.01	0.9107	
		0.25 g/L	0.003	0.9598	0.00009	0.9312	0.003	0.979	
		0.5 g/L	0.004	0.9631	0.0001	0.9296	0.003	0.973	
5	Dose	0.75 g/L	0.006	0.9563	0.0002	0.8744	0.006	0.966	
		1 g/L	0.009	0.9451	0.0004	0.8205	0.008	0.985	
		1.5 g/L	0.003	0.9252	0.00007	0.8893	0.002	0.965	

3.4.7. Comparative Studies for Degradation of Methyl Orange

In literature, innumerable studies have been reported for the photocatalytic degradation of dyes, where variety of heterostructures have generated remarkable dye degradations efficiencies. Here in the **table 3.2**, few of studies from published literature are cited to generate a comparative idea about the photocatalytic dye mineralization.

Nanomaterial Type	Dye Type and Concentration	Irradiation Source	Percentage Degradation/Reaction Time	Literature
15%BiVO ₄ @HMT.g-C ₃ N ₄	MO 50ppm	Visible Light	79.32%/180 min	This Study
Ag ₃ PO ₄ /Ti-BDC/g-C ₃ N ₄	MO 10ppm	Visible Light	99%/60 min	(Yassin et al., 2022)
PES-Ag ₃ PO ₄ /g-C ₃ N ₄ Film	MO 30ppm	Visible light	100%/60 min	(Mukhair et al., 2021)
10wt% g-C ₃ N ₄ /ZnS	MO 30ppm	Visible light	93.0 %/100 min	(Wang et al., 2020)
Bi ₂ O ₃ / BiVO ₄	MO 5ppm	Visible Light	97%/120 min	(Wu et al., 2016)
Bi ₂ MoO ₆ /TiO ₂	MO 10ppm	Visible Light	96%/100 min	(Zhang et al., 2015)
TiO ₂ P25	MO 5ppm	Visible Light	75%/ 180 min	(Regraguy et al., 2022)
10wt% g-C ₃ N ₄ /ZnS	MO 30ppm	Visible light	93.0 %/100 min	(Wang et al., 2020)

Table 3.2. Comparison of catalyst activities for MO dye degradation from literature

CONCLUSION

The decreased availability of drinkable water is diminishing rapidly due to toxic waste supplied by industries. This study presents heterogeneous photocatalysis for treatment of methyl orange dye contaminated water in simulated conditions. The methodology employed involved preliminary testing of various photocatalysts, including pristines, binary composites, and ternary composites. Among pristines; BiVO₄, HMT, g-C₃N₄, and different composite weight percentages synthesized as 5%, 10%, 15%, 20%, and 25%; 15% (BiVO₄@HMT/g-C₃N₄) achieved highest degradation rate. The optimization experiments were designed to determine the optimal pH, composite dose, and dye concentration. The degradation rate of methyl orange reached to 79.32% in 180min duration under irradiation of visible light, dose of VLA catalyst 1 g/L and pH 5 of solution. Moreover, the composite demonstrated reusability over three consecutive cycles, with the third run still retaining approximately 70% degradation efficiency. Catalytic photodegradation of MO dye followed the pseudo first order kinetics model which depicted that the reaction rate of ternary composite increased (0.003 min⁻¹ to 0.009⁻¹) 15% loading in heterostructure. The enhanced performance of the ternary composite (15%BiVO₄@HMT/g-C₃N₄) compared to pristine g-C₃N₄ confirmed the successful enhancement of the photocatalytic activity of g-C₃N₄.

This study's novelty lies in its investigation of the ternary composite and its effectiveness in dye degradation, as this composite has not been explored in previous research. These promising results pave the way for further exploration and optimization of composite structures, as well as their potential application to other toxic dyes removal. The insights gained from this study can envisage a future marked by innovative and sustainable solutions with potential to revolutionize wastewater treatment practices, fostering cleaner environments and healthier ecosystems.

REFERENCES

- Aljuaid, A., Almeahmadi, M., Alsaiari, A. A., Allahyani, M., Abdulaziz, O., Alsharif, A., Alsaiari, J., Salih, M. M., Alotaibi, R. T., & Khan, I. (2023). G-C₃N₄ based photocatalyst for the efficient photodegradation of toxic methyl orange dye: recent modifications and future perspectives. *Molecules*, *28*(7), 3199. <https://doi.org/10.3390/molecules28073199>
- Anusuyadevi, P. R. (2018). Synthesis of Novel Nanophotocatalyst in Micro/Millifluidic Supercritical Reactor (Doctoral dissertation, Université de Bordeaux).
- Arslan, M., Yaqub, M., & Shaikh, I. A. (2023). Assessment of reuse potential of highway runoff water in textile wet processing. *Water Resources and Industry*, 100222. <https://doi.org/10.1016/j.wri.2023.100222>
- Arun, J., Nachiappan, S., Rangarajan, G., Alagappan, R. P., Gopinath, K. P., & Lichtfouse, E. (2022). Synthesis and application of titanium dioxide photocatalysis for energy, decontamination and viral disinfection: a review. *Environmental Chemistry Letters*, *21*(1), 339–362. <https://doi.org/10.1007/s10311-022-01503-z>
- Ayele, A., Getachew, D., Kamaraj, M., & Suresh, A. (2021). Phycoremediation of Synthetic Dyes: An effective and Eco-Friendly algal technology for the dye abatement. *Journal of Chemistry*, *2021*, 1–14. <https://doi.org/10.1155/2021/9923643>
- Azanaw, A., Birlie, B., Teshome, B., & Jemberie, M. (2022). Textile effluent treatment methods and eco-friendly resolution of textile wastewater. *Case Studies in Chemical and Environmental Engineering*, *6*, 100230. <https://doi.org/10.1016/j.cscee.2022.100230>
- Bal, G., & Thakur, A. (2022). Distinct approaches of removal of dyes from wastewater: A review. *Materials Today: Proceedings*, *50*, 1575–1579. <https://doi.org/10.1016/j.matpr.2021.09.119>
- Behzadifard, Z., Shariatnia, Z., & Jourshabani, M. (2018). Novel visible light driven CuO/SmFeO₃ nanocomposite photocatalysts with enhanced photocatalytic activities for degradation of organic pollutants. *Journal of Molecular Liquids*, *262*, 533-548.
- Bhattacharjee, N., Som, I., Saha, R., & Mondal, S. (2022). A critical review on novel eco-friendly green approach to synthesize zinc oxide nanoparticles for photocatalytic

- degradation of water pollutants. *International Journal of Environmental Analytical Chemistry*, 1–28.
- Bota, S., & Indrie, L. (2021). Natural Dye Extraction and Dyeing of Different Fibers: A Review. *Innovative and Emerging Technologies for Textile Dyeing and Finishing*, 113–135. <https://doi.org/10.1002/9781119710288.ch4>
- Castillo-Suárez, L. A., Sierra-Sánchez, A. G., Linares-Hernández, I., Martínez-Miranda, V., & Teutli-Sequeira, E. A. (2023). A critical review of textile industry wastewater: green technologies for the removal of indigo dyes. *International Journal of Environmental Science and Technology*, 20(9), 10553–10590.
- Chang, F., Xie, Y., Li, C., Chen, J., Luo, J., Hu, X., & Shen, J. (2013). A facile modification of g-C₃N₄ with enhanced photocatalytic activity for degradation of methylene blue. *Applied Surface Science*, 280, 967-974.
- Chen, T., Quan, W., Yu, L., Hong, Y., Song, C., Fan, M., ... & Shi, W. (2016). One-step synthesis and visible-light-driven H₂ production from water splitting of Ag quantum dots/g-C₃N₄ photocatalysts. *Journal of Alloys and Compounds*, 686, 628-634.
- Dinar, A., Tieu, A., & Huynh, H. (2019b). Water scarcity impacts on global food production. *Global Food Security*, 23, 212–226. *Engineering*, 10(3), 107549. <https://doi.org/10.1016/j.jece.2022.107549>
- Fu, J., Wang, Y., Jiang, C., & Cheng, B. (2017). g-C₃N₄-Based Heterostructured Photocatalysts. *Advanced Energy Materials*, 8(3). <https://doi.org/10.1002/aenm.201701503>
- George, J., Rajendran, D. S., Kumar, P. S., Anand, S. S., Kumar, V. V., & Rangasamy, G. (2023). Efficient decolorization and detoxification of triarylmethane and azo dyes by porous-cross-linked enzyme aggregates of *Pleurotus ostreatus* laccase. *Chemosphere*, 313, 137612.
- Guo, R., Wang, J., Bi, Z., Chen, X., Hu, X., & Pan, W. (2022). Recent advances and perspectives of g-C₃N₄-based materials for photocatalytic dyes degradation. *Chemosphere*, 295, 133834. <https://doi.org/10.1016/j.chemosphere.2022.133834>
- Guo, Y., Wang, R., Wang, P., Li, Y., & Wang, C. (2017). Developing polyetherimide/graphitic carbon nitride floating photocatalyst with good photodegradation performance of methyl

- orange under light irradiation. *Chemosphere*, 179, 84–91.
<https://doi.org/10.1016/j.chemosphere.2017.03.085>
- Hakami, A. a. H., Wabaidur, S. M., Khan, M. A., ALOthman, Z. A., & Siddiqui, M. R. (2021). Extraction Procedures and Analytical Methods for the Determination of Methylene Blue, Rhodamine B and Crystal Violet - An Overview. *Current Analytical Chemistry*, 17(5), 708–728. <https://doi.org/10.2174/1573411017999201125203536>
- Han, E., K. Vijayarangamuthu, Youn, J.-C., Park, Y.-K., Jung, S.-C., & Jeon, K.-J. (2018). Degussa P25 TiO₂ modified with H₂O₂ under microwave treatment to enhance photocatalytic properties. *Catalysis Today*, 303, 305–312.
- Hanafī, M. F., & Sapawe, N. (2020). A review on the water problem associate with organic pollutants derived from phenol, methyl orange, and remazol brilliant blue dyes. *Materials Today: Proceedings*, 31, A141-A150.
- Hanif, Md. A., Akter, J., Kim, Y. S., Kim, H. G., Hahn, J. R., & Kwac, L. K. (2022). Highly Efficient and Sustainable ZnO/CuO/g-C₃N₄ Photocatalyst for Wastewater Treatment under Visible Light through Heterojunction Development. *Catalysts*, 12(2), 151.
- Helaimia, R. (2023). CONDENSATION, DESALINATION, AND WATER RECYCLING TO ENCOUNTER WATER STRESS. *International Conference on Pioneer and Innovative Studies*, 1, 515–523. <https://doi.org/10.59287/icpis.883>
<https://doi.org/10.1007/s13762-023-04810-2>
- Idris, N. H. M., Cheong, K. Y., Kennedy, B. J., Ohno, T., & Lee, H. L. (2022). Buoyant titanium dioxide (TiO₂) as high performance photocatalyst and peroxide activator: A critical review on fabrication, mechanism and application. *Journal of Environmental Chemical*
- Ingrassia, E. B., Lemos, E. S., & Escudero, L. B. (2023). Treatment of textile wastewater using carbon-based nanomaterials as adsorbents: a review. *Environmental Science and Pollution Research*, 30(40), 91649–91675. <https://doi.org/10.1007/s11356-023-28908-9>
- Isaev, A. B., Shabanov, N. S., Magomedova, A., Nidheesh, P., & Oturan, M. A. (2023). Electrochemical oxidation of azo dyes in water: a review. *Environmental Chemistry Letters*. <https://doi.org/10.1007/s10311-023-01610-5>
- Islam, M. N., Kumar, S., Saxena, N., & Nafees, A. (2023). Photocatalytic degradation of dyes present in industrial effluents: a review. *ChemistrySelect*, 8(26).
<https://doi.org/10.1002/slct.202301048>

- Iwuozor, K. O., Ighalo, J. O., Emenike, E. C., Ogunfowora, L. A., & Igwegbe, C. A. (2021). Adsorption of methyl orange: A review on adsorbent performance. *Current Research in Green and Sustainable Chemistry*, 4, 100179. <https://doi.org/10.1016/j.crgsc.2021.100179>
- Kaczorowska, M. A., Bożejewicz, D., & Witt, K. (2023). The Application of Polymer Inclusion Membranes for the Removal of Emerging Contaminants and Synthetic Dyes from Aqueous Solutions—A Mini Review. *Membranes*, 13(2), 132. <https://doi.org/10.3390/membranes13020132>
- Kamble, G. S., Natarajan, T. S., Patil, S. S., Thomas, M., Chougale, R. K., Sanadi, P., Siddharth, U. S., & Ling, Y. (2023). BiVO₄ As a Sustainable and Emerging Photocatalyst: Synthesis Methodologies, Engineering Properties, and Its Volatile Organic Compounds Degradation Efficiency. *Nanomaterials*, 13(9), 1528. <https://doi.org/10.3390/nano13091528>
- Kang, S. (2017). Hydrogen peroxide activated commercial P25 TiO₂ as efficient visible-light-driven photocatalyst on dye degradation. *International Journal of Electrochemical Science*, 5284–5293. <https://doi.org/10.20964/2017.06.54>
- Lekhak, U. M. (2023). Ecotoxicity of synthetic dyes. In *Elsevier eBooks* (pp. 45–67). <https://doi.org/10.1016/b978-0-323-91235-8.00021-8>
- Liu, C., & Perng, T. (2020). Fabrication and band structure of Ag₃PO₄–TiO₂ heterojunction with enhanced photocatalytic hydrogen evolution. *International Journal of Hydrogen Energy*, 45(1), 149–159. <https://doi.org/10.1016/j.ijhydene.2019.10.182>
- Liu, H., Zhang, Z., He, H., Wang, X., Zhang, J., Zhang, Q., Tong, Y., Liu, H., Ramakrishna, S., Shi, Y., & Long, Y. (2018). One-Step synthesis heterostructured g-C₃N₄/TiO₂ composite for rapid degradation of pollutants in utilizing visible light. *Nanomaterials*, 8(10), 842. <https://doi.org/10.3390/nano8100842>
- Liu, J., Luo, Z., Mao, X., Dong, Y., Peng, L., Sun-Waterhouse, D., Kennedy, J., & Waterhouse, G. I. (2022). Recent advances in Self-Supported semiconductor heterojunction

- nanoarrays as efficient photoanodes for photoelectrochemical water splitting. *Small*, 18(48), 2204553. <https://doi.org/10.1002/sml.202204553>
- Liu, S., Tang, H., Zhou, H., Dai, G., & Wang, W. (2017). Photocatalytic performance of sandwich-like BiVO₄ sheets by microwave assisted synthesis. *Applied Surface Science*, 391, 542–547. <https://doi.org/10.1016/j.apsusc.2016.06.184>
- Longchin, P., Pookmanee, P., Satienerakul, S., Sangsrichan, S., Puntharod, R., Kruefu, V., Kangwansupamonkon, W., & Phanichphant, S. (2016). Characterization of bismuth vanadate (BiVO₄) nanoparticle prepared by solvothermal method. *Integrated Ferroelectrics*, 175(1), 18–24. <https://doi.org/10.1080/10584587.2016.1199845>
- Lotfi, S., Ouardi, M. E., Ahsaine, H. A., & Assani, A. (2022). Recent progress on the synthesis, morphology and photocatalytic dye degradation of BiVO₄ photocatalysts: A review. *Catalysis Reviews-science and Engineering*, 1–45. <https://doi.org/10.1080/01614940.2022.2057044>
- Ma, D., Wu, J., Gao, M., Xin, Y., Ma, T., & Sun, Y. (2016). Fabrication of Z-scheme g-C₃N₄/RGO/Bi₂WO₆ photocatalyst with enhanced visible-light photocatalytic activity. *Chemical Engineering Journal*, 290, 136-146.
- Malviya, A., Jaspal, D., Sharma, P., & Dubey, A. (2015). Isothermal mathematical modeling for decolorizing water-A comparative approach. *Sustainable Environment Research*, 25(1).
- Mane, P., Bae, H., Burungale, V., Lee, S., Misra, M., Parbat, H., Kadam, A. N., & Ha, J. (2022). Interface-engineered Z-scheme of BiVO₄/g-C₃N₄ photoanode for boosted photoelectrochemical water splitting and organic contaminant elimination under solar light. *Chemosphere*, 308, 136166. <https://doi.org/10.1016/j.chemosphere.2022.136166>
- Meurs, E. (2023). *Study on Decolourization of Reactive-dyed Cotton through Fenton-oxidation as a Pre-treatment for Textile Recycling*. DIVA. <https://www.diva-portal.org/smash/record.jsf?pid=diva2:1777802>
- Mishra, R. (2023). Fresh Water availability and Its Global challenge. *British Journal of Multidisciplinary and Advanced Studies*, 4(3), 1–78. <https://doi.org/10.37745/bjmas.2022.0208>

- Nabi, G., Ali, M., Khan, S., & Kumar, S. (2019). The crisis of water shortage and pollution in Pakistan: risk to public health, biodiversity, and ecosystem. *Environmental Science and Pollution Research*, 26(11), 10443–10445. <https://doi.org/10.1007/s11356-019-04483-w>
- Nagarajan, K., Surumbarkuzhali, N., & Parimala, K. (2023). Vibrational dynamics, Hirshfeld surface and molecular docking studies by quantum computational analysis of 3-Hydroxy-4-nitrobenzaldehyde. *Phase Transitions*, 1–23. <https://doi.org/10.1080/01411594.2023.2249197>
- Naikwade, A., Jagadale, M., Kale, D., Gophane, A., Garadkar, K. M., & Rashinkar, G. (2020). Photocatalytic degradation of methyl orange by magnetically retrievable supported ionic liquid phase photocatalyst. *ACS Omega*, 5(1), 131–144. <https://doi.org/10.1021/acsomega.9b02040>
- Nipun, N. J. (2023, July 20). *Sustainable Innovation for Reducing Negative Environmental Impact in the Textile Industry - A Comparative Case Study Between Sweden and Bangladesh*. <https://gupea.ub.gu.se/handle/2077/77887>
- Noreen, M., & Younes, I. (2023). Wastewater irrigation and its impact on crops in major cultivated belt of Rechna doab, Pakistan. *Kuwait Journal of Science*. <https://doi.org/10.1016/j.kjs.2023.08.003>
- Norouzzadeh, P., Mabhouti, K., Golzan, M. M., & Naderali, R. (2020). Consequence of Mn and Ni doping on structural, optical and magnetic characteristics of ZnO nanopowders: the Williamson–Hall method, the Kramers–Kronig approach and magnetic interactions. *Applied Physics A*, 126, 1-13.,
- Onwudiwe, D. C., Phadi, B. M., & Oyewo, O. A. (2021). Ce₂O₃/BiVO₄ Embedded in rGO as Photocatalyst for the Degradation of Methyl Orange under Visible Light Irradiation. *J*, 4(2), 154–168. <https://doi.org/10.3390/j4020013>
- Pasdaran, A., Zare, M., Hamedi, A., & Hamedi, A. (2023). A review of the chemistry and biological activities of natural colourants, dyes, and pigments: challenges, and opportunities for food, cosmetics, and pharmaceutical application. *Chemistry & Biodiversity*, 20(8). <https://doi.org/10.1002/cbdv.202300561>

- Phadi, B. M., Oyewo, O. A., Ramaila, S., Mavuru, L., & Onwudiwe, D. C. (2021). Nanocomposite of CEVO₄/BIVO₄ loaded on reduced graphene oxide for the photocatalytic degradation of methyl orange. *Journal of Cluster Science*, 33(6), 2707–2721. <https://doi.org/10.1007/s10876-021-02189-z>
- Pookmanee, P., Kojinok, S., Puntharod, R., Sangsrichan, S., & Phanichphant, S. (2013). Preparation and Characterization of BiVO₄ Powder by the Sol-gel Method. *Ferroelectrics*, 456(1), 45–54. <https://doi.org/10.1080/00150193.2013.846197>
- Pratiwi, D., Prasetyo, D. J., & Poeloengasih, C. D. (2019). Adsorption of Methylene Blue dye using Marine algae *Ulva lactuca*. *IOP Conference Series*, 251, 012012. <https://doi.org/10.1088/1755-1315/251/1/012012>
- PubChem. (n.d.). PubChem. PubChem. <https://pubchem.ncbi.nlm.nih.gov/>
- Rajaitha, P. M., Hajra, S., Sahu, M., Mistewicz, K., Toroń, B., Abolhassani, R., Panda, S. S., Mishra, Y. K., & Kim, H. J. (2022). Unraveling highly efficient nanomaterial photocatalyst for pollutant removal: a comprehensive review and future progress. *Materials Today Chemistry*, 23, 100692. <https://doi.org/10.1016/j.mtchem.2021.100692>
- Ramireddy, V. S. R., Kurakula, R., Chellam, P. V., James, A., & Van Hullebusch, E. D. (2023). Systematic computational toxicity analysis of the ozonolytic degraded compounds of azo dyes: Quantitative structure-activity relationship (QSAR) and adverse outcome pathway (AOP) based approach. *Environmental Research*, 231, 116142. <https://doi.org/10.1016/j.envres.2023.116142>
- Rashid, J., Imtiaz, F., Xu, M., & Savina, I. N. (2022). Hydrogen peroxide modified and bismuth vanadate decorated titanium dioxide nanocomposite (BiVO₄@HMT) for enhanced visible light photocatalytic growth inhibition of harmful cyanobacteria in water. *RSC Advances*, 12(48), 31338–31351. <https://doi.org/10.1039/d2ra05317a>
- Regraguy, B., Rahmani, M., Mabrouki, J., Drhimer, F., Ellouzi, I., Mahmoud, C., Dahchour, A., Mrabet, M. E., & Hajjaji, S. E. (2022). Photocatalytic degradation of methyl orange in the presence of nanoparticles NiSO₄/TiO₂. *Nanotechnology for Environmental Engineering*, 7(1), 157–171. <https://doi.org/10.1007/s41204-021-00206-0>

- Sajid, M. M., Khan, S. B., Javed, Y., Amin, N., Zhang, Z., Shad, N. A., & Zhai, H. (2021). Bismuth vanadate/MXene (BiVO₄/Ti₃C₂) heterojunction composite: enhanced interfacial control charge transfer for highly efficient visible light photocatalytic activity. *Environmental Science and Pollution Research*, 28(27), 35911–35923. <https://doi.org/10.1007/s11356-021-13315-9>
- Selvaraj, V., Karthika, T., C, M., & Alagar, M. (2021). An over review on recently developed techniques, mechanisms and intermediate involved in the advanced azo dye degradation for industrial applications. *Journal of Molecular Structure*, 1224, 129195. <https://doi.org/10.1016/j.molstruc.2020.129195>
- Seow, T. W., Lim, C. K., Nor, M. H. M., Mubarak, M. F. M., Lam, C. Y., Yahya, A., & Ibrahim, Z. (2016). Review on wastewater treatment technologies. *Int. J. Appl. Environ. Sci*, 11(1), 111-126.
- Shafiq, F., Muhammad Bilal Tahir, Hussain, A., Muhammad Sagir, Jalil Ur Rehman, Imen Kebaili, Hussein Alrobei, & Meshal Alzaid. (2022). The construction of a highly efficient p-n heterojunction Bi₂O₃/BiVO₄ for hydrogen evolution through solar water splitting. *International Journal of Hydrogen Energy*, 47(7), 4594–4600.
- Sharma, J., Sharma, S., & Soni, V. (2021). Classification and impact of synthetic textile dyes on Aquatic Flora: A review. *Regional Studies in Marine Science*, 45, 101802. <https://doi.org/10.1016/j.rsma.2021.101802>
- Shemer, H., Wald, S., & Semiat, R. (2023). Challenges and solutions for global water scarcity. *Membranes*, 13(6), 612. <https://doi.org/10.3390/membranes13060612>
- Slama, H. B., Bouket, A. C., Pourhassan, Z., Alenezi, F. N., Silini, A., Cherif-Silini, H., Oszako, T., Luptakova, L., Golińska, P., & Belbahri, L. (2021). Diversity of Synthetic Dyes from Textile Industries, Discharge Impacts and Treatment Methods. *Applied Sciences*, 11(14), 6255. <https://doi.org/10.3390/app11146255>
- Srivastava, A., Rani, R., Patle, D. S., & Kumar, S. (2021). Emerging bioremediation technologies for the treatment of textile wastewater containing synthetic dyes: a comprehensive review. *Journal of Chemical Technology & Biotechnology*, 97(1), 26–41. <https://doi.org/10.1002/jctb.6891>

- Sudarshan, S., Harikrishnan, S., RathiBhuvaneswari, G., Alamelu, V., Aanand, S., Rajasekar, A., & Govarthanan, M. (2022). Impact of textile dyes on human health and bioremediation of textile industry effluent using microorganisms: current status and future prospects. *Journal of Applied Microbiology*, 134(2). <https://doi.org/10.1093/jambio/lxac064>
- Tadesse, S. F., Kuo, D. H., Kebede, W. L., & Wolde, G. S. (2021). Visible light driven Nd₂O₃/Mo (S, O) 3-x·0.34 H₂O heterojunction for enhanced photocatalytic degradation of organic pollutants. *Applied Surface Science*, 569, 151091.
- Tan, L., Xu, J., Zhang, X., Hang, Z., Jia, Y., & Wang, S. (2015). Synthesis of g-C₃N₄/CeO₂ nanocomposites with improved catalytic activity on the thermal decomposition of ammonium perchlorate. *Applied Surface Science*, 356, 447-453.
- Tatarchuk, Tetiana & Peter, Amalathi & Al-Najar, Basma & Vijaya, Judith & Bououdina, Mohamed.(2018). Photocatalysis: Activity of Nanomaterials. 10.1002/9783527808854.
- Tkaczyk, A., Mitrowska, K., & Posyniak, A. (2020). Synthetic organic dyes as contaminants of the aquatic environment and their implications for ecosystems: A review. *Science of the Total Environment*, 717, 137222. <https://doi.org/10.1016/j.scitotenv.2020.137222>
- Uddin, M. K., & Rehman, Z. (2018). Application of Nanomaterials in the Remediation of Textile Effluents from Aqueous Solutions. In *John Wiley & Sons, Inc. eBooks* (pp. 135–161). <https://doi.org/10.1002/9781119459804.ch4>
- Vaiano, V., & De Marco, I. (2023a). Removal of Azo Dyes from Wastewater through Heterogeneous Photocatalysis and Supercritical Water Oxidation. *Separations*, 10(4), 230. <https://doi.org/10.3390/separations10040230>
- Waghchaure, R. H., Adole, V. A., & Jagdale, B. S. (2022). Photocatalytic degradation of methylene blue, rhodamine B, methyl orange and Eriochrome black T dyes by modified ZnO nanocatalysts: A concise review. *Inorganic Chemistry Communications*, 143, 109764. <https://doi.org/10.1016/j.inoche.2022.109764>
- Wang, H., Li, X., Zhao, X., Li, C., Song, X., Zhang, P., Huo, P., & Li, X. (2022a). A review on heterogeneous photocatalysis for environmental remediation: From semiconductors to modification strategies. *Chinese Journal of Catalysis*, 43(2), 178–214. [https://doi.org/10.1016/s1872-2067\(21\)63910-4](https://doi.org/10.1016/s1872-2067(21)63910-4)

- Wang, L., Jiang, J., Ma, J., Pang, S., & Zhang, T. (2022b). A review on advanced oxidation processes homogeneously initiated by copper(II). *Chemical Engineering Journal*, 427, 131721. <https://doi.org/10.1016/j.cej.2021.131721>
- Xi-Jun, M., Zhou, Y., Gu, S., Su, M., Zhu, G., Yu, M., Wu, Y., Ping, Y., Hong, K., Zhang, J., Mao, P., & Wu, Z. (2022). Degradation of hexavalent chromium and methyl orange by the synergistic system of graphitic carbon nitride and electron beam irradiation. *Chemosphere*, 287, 132228.
- Yadav, B. S., & Dasgupta, S. (2022). Effect of time, pH, and temperature on kinetics for adsorption of methyl orange dye into the modified nitrate intercalated MgAl LDH adsorbent. *Inorganic Chemistry Communications*, 137, 109203. <https://doi.org/10.1016/j.inoche.2022.109203>
- Yang, J., Chen, H., Gao, J., Yan, T., Zhou, F., Cui, S., & Bi, W. (2016). Synthesis of Fe₃O₄/g-C₃N₄ nanocomposites and their application in the photodegradation of 2, 4, 6-trichlorophenol under visible light. *Materials Letters*, 164, 183-189.
- Yang, L., Huang, J., Shi, L., Cao, L., Yu, Q., Jie, Y., ... & Ye, J. (2017). A surface modification resultant thermally oxidized porous g-C₃N₄ with enhanced photocatalytic hydrogen production. *Applied Catalysis B: Environmental*, 204, 335-345.
- Ying, Y., Tao, F., Hong, T., & Wang, L. (2015). Controlled fabrication of bismuth vanadium oxide hierarchical microtubes with enhanced visible light photocatalytic activity. *Materials Science in Semiconductor Processing*, 32, 82–89. <https://doi.org/10.1016/j.mssp.2015.01.009>
- Younis, S. A., & Kim, K. (2020). Heterogeneous Photocatalysis Scalability for Environmental Remediation: Opportunities and challenges. *Catalysts*, 10(10), 1109. <https://doi.org/10.3390/catal10101109>
- Zeghioud, H., Khellaf, N., Amrane, A., Djelal, H., Bouhelassa, M., Assadi, A. A., & Rtimi, S. (2020). Combining photocatalytic process and biological treatment for Reactive Green 12 degradation: optimization, mineralization, and phytotoxicity with seed germination. *Environmental Science and Pollution Research*, 28(10), 12490–12499. <https://doi.org/10.1007/s11356-020-11282-1>

- Zhang, Y., & Li, G. (2020). Recent advances of Epitaxial BiVO₄ Thin film: Preparation and physical and photoelectrochemical properties. *Brazilian Journal of Physics*, 50(2), 185–191. <https://doi.org/10.1007/s13538-019-00730-0>
- Zhang, Y., Pan, Q., Chai, G., Liang, M., Dong, G., Zhang, Q., & Qiu, J. (2013). Synthesis and luminescence mechanism of multicolour-emitting g-C₃N₄ nanopowders by low temperature thermal condensation of melamine. *Scientific Reports*, 3(1). <https://doi.org/10.1038/srep01943>
- Zhao, J., Yan, J., Jia, H., Zhong, S., Zhang, X., & Xu, L. (2016). BiVO₄/g-C₃N₄ composite visible-light photocatalyst for effective elimination of aqueous organic pollutants. *Journal of Molecular Catalysis A-chemical*, 424, 162–170. <https://doi.org/10.1016/j.molcata.2016.08.025>
- Zhu, Y. P., Li, M., Liu, Y. L., Ren, T. Z., & Yuan, Z. Y. (2014). Carbon-doped ZnO hybridized homogeneously with graphitic carbon nitride nanocomposites for photocatalysis. *The Journal of Physical Chemistry C*, 118(20), 10963-10971.
- Zou, L., Wang, H., & Wang, X. (2016). High Efficient Photodegradation and Photocatalytic Hydrogen Production of CdS/BiVO₄ Heterostructure through Z-Scheme Process. *ACS Sustainable Chemistry & Engineering*, 5(1), 303–309. <https://doi.org/10.1021/acssuschemeng.6b01628>

Waqar Alam Thesis Similarity 15-9-2023

ORIGINALITY REPORT

11 %	7 %	9 %	4 %
SIMILARITY INDEX	INTERNET SOURCES	PUBLICATIONS	STUDENT PAPERS

PRIMARY SOURCES

1	www.ncbi.nlm.nih.gov Internet Source	2 %
2	Submitted to Higher Education Commission Pakistan Student Paper	1 %
3	Muhammad Farhan Hanafi, Norzahir Sapawe. "Influence of pH on the photocatalytic degradation of methyl orange using nickel catalyst", Materials Today: Proceedings, 2020 Publication	1 %
4	Jamshaid Rashid, Ali Ahsan, Ming Xu, Irina Savina, Faisal Rehman. "Synthesis of cerium oxide embedded perovskite type bismuth ferrite nanocomposites for sonophotocatalysis of aqueous micropollutant ibuprofen", RSC Advances, 2023 Publication	1 %
5	Safia Lotfi, Mohamed El Ouardi, Hassan Ait Ahsaine, Abderrazzak Assani. " Recent progress on the synthesis, morphology and	<1 %